JAM-2: Fully computational design of drug-like antibodies with high success rates

Nabla Bio

Abstract

We present JAM-2, a general-purpose *de novo* protein design system that for the first time yields VHH-Fc and full-length mAb antibodies with drug-like affinities and developability, while achieving double-digit success rates with unprecedented target and epitope breadth. Across 16 unseen targets, JAM-2 produced binders for 100% of them, with average success rates of 39% (VHH-Fcs) and 18% (mAbs). Using only 45 designs per format, JAM-2 delivered picomolar or single-digit nanomolar binders on half of these targets. Across another 10 targets, each with 20 user-specified epitopes, JAM-2 generated VHH-Fc binders to 30–70% of epitopes for half the targets. Remarkably, JAM-2 also produced antibody binders directly to the GPCRs CXCR4 and CXCR7 in their native cellular contexts with 11.7% and 3.8% success rates, respectively, with top designs reaching single-digit nanomolar affinities. Developability profiling of hundreds of *de novo* designs — the largest developability dataset for computationally designed biologics — showed more than half met core industry criteria, with many top designs exhibiting lead-quality profiles that may not require further optimization of any kind. These results position JAM-2 as the state-of-the-art *de novo* antibody design system, and the first ready for front-line use in drug discovery, matching or surpassing traditional discovery approaches.

Introduction

Antibodies are among the most successful therapeutic modalities, accounting for more than 100 approved drugs and over half of all biologics entering clinical development^{1–3}. Their modularity, potency, and long serum half-life make them central to interventions across oncology, immunology, infectious disease, and rare disorders. Despite this impact, the discovery process remains slow and labor-intensive. Immunization and display technologies routinely require screening billions of variants, multiple enrichment rounds, and target-specific optimization, and their success remains uneven across difficult epitopes and challenging classes such as GPCRs, ion channels, and multipass receptors^{4–6}.

A long-standing goal has been to replace this stochastic search with *de novo* design – directly generating antibodies that bind a specified epitope, in a desired orientation, with drug-like biophysical properties without using information from a known binder. Such a capability would broaden what can be targeted, enabling ligands to orthosteric pockets of GPCRs, quaternary interfaces, post-translational modifications, and other regions that are poorly represented or inaccessible in host immunity and display libraries. It would also enable control over functional outcomes (antagonism, agonism, biased signaling, internalization) by intentionally designing the geometry of recognition. Equally important, computational design would allow parallel discovery across many targets, reducing experimental load and accelerating hypothesis testing in early drug development.

Recent generative approaches have moved the field toward this vision. RFAntibody⁷, Chai-2⁸, Germinal⁹, mBER¹⁰, and BoltzGen¹¹ each demonstrated *de novo* generation of binders *in vitro* without relying on existing antibodies. These studies represent meaningful progress: they report double-digit hit rates on soluble targets, occasional nanomolar affinities, and modest demonstrations of epitope conditioning. But the resulting antibodies commonly exhibit high-nanomolar affinities that would require substantial optimization in the context of drug discovery, are tested under permissive or non-standard assay conditions, and provide limited data on developability or specificity. Epitope coverage is narrow, and – with the exception of our previous work^{12,13} – applications have been restricted to relatively tractable soluble proteins that do not challenge traditional discovery. In aggregate, these approaches have not yet achieved the reliability, affinity, epitope breadth, or developability required to offer a strong advantage over established immunization or display workflows.

Here we introduce JAM-2, a generative biomolecular design system that addresses these gaps. Using a unified, fully computational design workflow, JAM-2 produces VHH-Fcs and full-length monoclonal antibodies (mAbs) with high success rates, low-nanomolar to sub-nanomolar affinities, and developability metrics comparable to late-clinical-stage or FDA-approved antibodies. Across 28 structurally and functionally diverse targets, JAM-2 achieves consistent double-digit hit rates from small design sets, under standardized assays and mammalian expression formats. It further generalizes to epitope-level design, reliably producing binders to 30-70% of intentionally selected epitopes on many targets. Finally, JAM-2 extends *de novo* design into classes that have historically resisted *in vitro* discovery, generating nanomolar,

epitope-specific antibodies directly against native GPCRs without proxy screening and with 3-11% success rates.

Importantly, all measurements were performed in our lab under conditions consistent with rigorous industry practice. Except for one target (TrkA), we did not use target proteins artificially multimerized by their expression tag, used sub-micromolar analyte concentrations and non-avid conditions during affinity assessments (unless otherwise noted, due to native multimerization of the receptor), and applied industry best-practice workflows across all targets and formats.

Together, these results show that *de novo* antibody design can now deliver molecules that meet the core requirements of early therapeutic discovery – affinity, specificity, epitope control, target breadth, and developability – while dramatically reducing experimental burden. In doing so, JAM-2 moves *de novo* antibody generation from a proof-of-principle capability to a reliable, industry-grade discovery engine.

Results

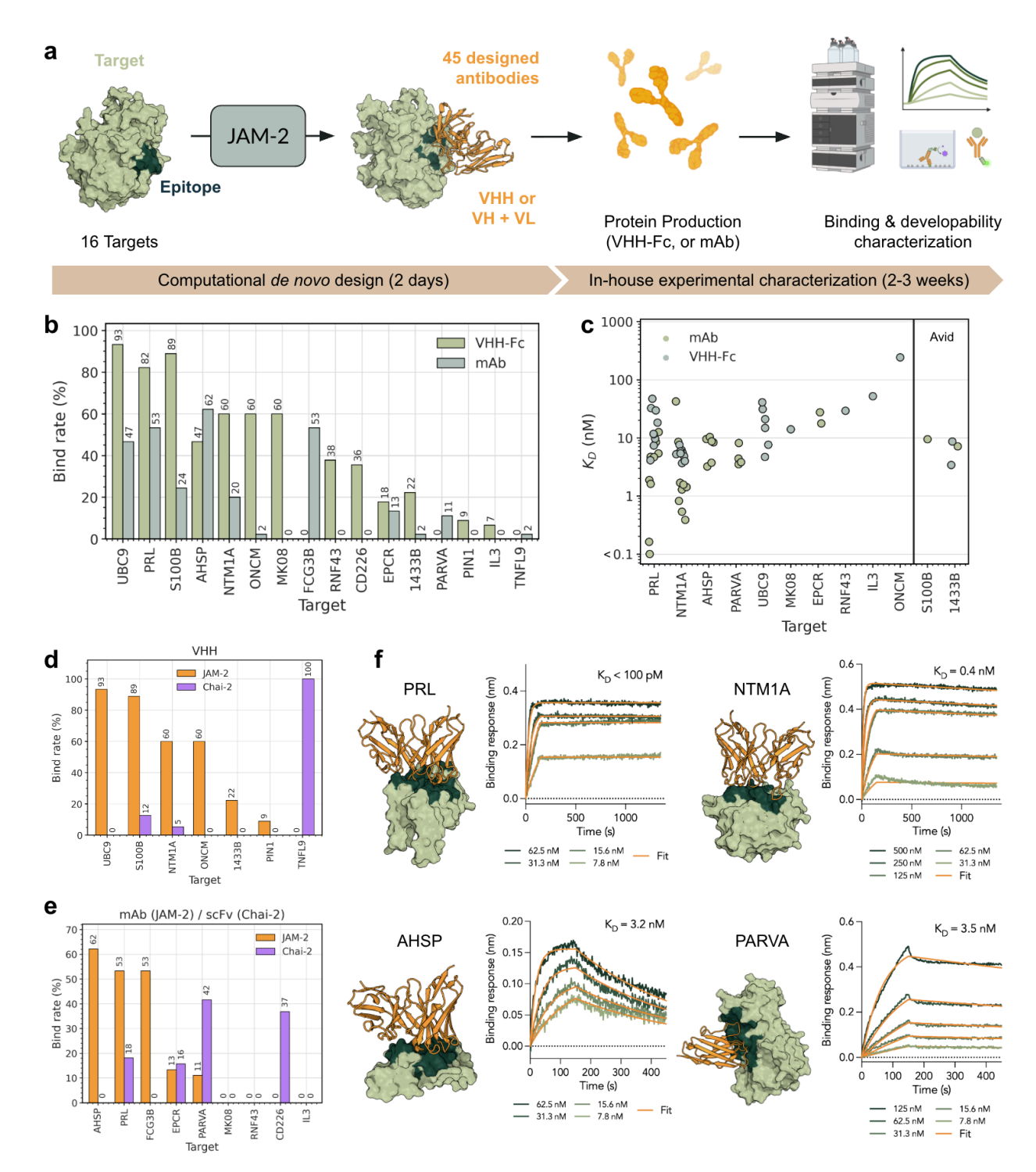


Figure 1: JAM-2 *de novo* designs antibodies with drug-like affinities to unseen targets and with double-digit bind rates. a. For each of 16 antigens, JAM-2 designs 45 antibodies per format (VHH or VH+VL), which are expressed as VHH-Fcs or full-length mAbs, purified, and subjected to binding and developability characterization. b. Per-target bind rates for VHH-Fcs (green) and mAbs (blue) in a binary BLI screen. c. Binding affinities of recombinant JAM-2–designed antibodies across targets, measured by BLI. Antibody binders for which an accurate K_D ($R^2 > 0.95$) was not calculable under these high-throughput conditions are excluded. The "Avid" group denotes designs whose binding is impacted by avidity effects that stem from natural antigen multimericity. For binders

with affinities marked at <100 pM, these had otherwise high quality sensorgrams, but we were not able to observe adequate dissociation in the assay conditions run to accurately measure their off-rate. However, it was clear the binder had <100 pM K_D . d. Comparison of VHH bind rates between JAM-2 designs (orange; expressed as VHH-Fc) and Chai-2 designs (purple; expressed as VHH) on the seven shared targets. e. Comparison of mAb bind rates between JAM-2 designs (orange; expressed as full-length mAb) and Chai-2 scFv designs (purple) on the nine shared targets. f. Cherry-picked *de novo* designed antibodies and corresponding BLI sensorgrams PRL, NTM1A, AHSP, and PARVA.

JAM-2 designs VHH-Fc and full-length mAbs with drug-like affinities across diverse, previously unseen targets

We first evaluated JAM-2 on targets completely unseen during training. These proteins had no close homology to any antibody–antigen complex available at the model's training cutoff. To facilitate benchmarking, we focused on 16 targets overlapping with the Chai-2 study, which reported outcomes ranging from complete failure to complete success. We refer to this group as Target Set 1 (Table 2).

JAM-2 produces ranked designs for each target and generates the full set of CDRs (IMGT definition), along with a small number of adjacent framework 2 and 3 residues that contact the antigen. We speculate that including these supporting framework residues helps stabilize the CDRs in their binding poses without detrimentally affecting humanness¹⁴.

For each target, JAM-2 generated 45 VHH variable domains and 45 paired VH+VL variable domains. These designs were then expressed as VHH-Fcs or full-length mAbs, respectively. All constructs were produced in ExpiCHO and screened for binary binding via biolayer interferometry (Methods, Supp. Fig. 1). JAM-2 produced binders for every target (Fig. 1b). Average per-target success rates (percent of designs that bound) were 39% for VHH-Fcs and 18% for mAbs, and the two formats showed complementary success patterns across antigens.

Affinity measurements for a subset of these 16 targets showed that JAM-2 produced picomolar binders for 2/16 targets, single-digit nanomolar affinities for 7/16 targets, and double-digit nanomolar affinities for 11/16 targets (Fig. 1c, Supp. Fig. 2). These numbers are conservative. First, many profiles were consistent with low-nanomolar binding but narrowly missed fit-quality thresholds, and we expect that modest, target-specific assay optimization – typical in industrial workflows – would recover many of these as passing (BLI sensorgrams are shared in the Suppl. Fig 2). Second, some attrition of binary binding and affinity is expected due to reformatting the designed VHH and VH+VL variable domains into VHH-Fc and full-length mAbs. Nevertheless, the high success rates we observe suggests reformatting is not a practical limitation, and in fact, that JAM-2 variable domain designs should be easily incorporated into non-standard antibody formats, like multispecifics.

Though VHH-Fcs showed higher bind rates, the best affinities were observed for mAbs (Fig. 1c). Both VHH-Fcs and mAbs yielded multiple single- or sub-nanomolar binders across antigens. This affinity range is comparable to what is typically obtained from display or immunization campaigns but here arises directly from computational design, without library screening or iterative lab-in-the-loop optimization, and from only 45 designs per format.

Among the 16 targets we selected, 7 were ones for which Chai-2 made VHH designs and 9 were ones for which Chai-2 made scFv designs. On the seven VHH targets, JAM-2 generated VHH-Fc binders for four targets where Chai-2 reported none and achieved higher success rates on two others (Fig. 1d); JAM-2 did not produce VHH-Fc binders to TNFL9, where Chai-2 reported a 100% success rate (Fig. 1d). We note TNFL9 is a trimeric antigen, and the construct used in the Chai-2 study was a TNFL9 monomer artificially dimerized with an Fc-tag without SEC verification, potentially forming an oligomeric, avid antigen and therefore potentially inflating hit rates.

For the 9 scFv (Chai-2) / mAb (JAM-2) targets, JAM-2 produced full-length mAb binders for five targets compared with four for Chai-2, with three shared successes (Fig. 1e). Crucially, when considering both formats together, JAM-2 produced binders to all 16 targets: every target lacking VHH-Fc binders was recovered by mAbs, and vice versa, underscoring complementary coverage across formats.

Representative structures and BLI profiles for top JAM-2 binders are shown in Figure 1e, highlighting CDR-driven interfaces consistent with typical antibody recognition.

This entire workflow covering 2 formats (mAb and VHH) and 16 independent targets, from initiating design to purified affinity measurements, was completed in under four weeks by a four-person team.

Taken together, these results show that designing variable domains and expressing them as VHH-Fcs or full-length mAbs can reliably yield antibodies with hit rates, affinity ranges, and biochemical quality comparable to state-of-the-art discovery platforms, but with far less experimental effort and across a broader and more diverse set of targets than traditional approaches typically sustain.

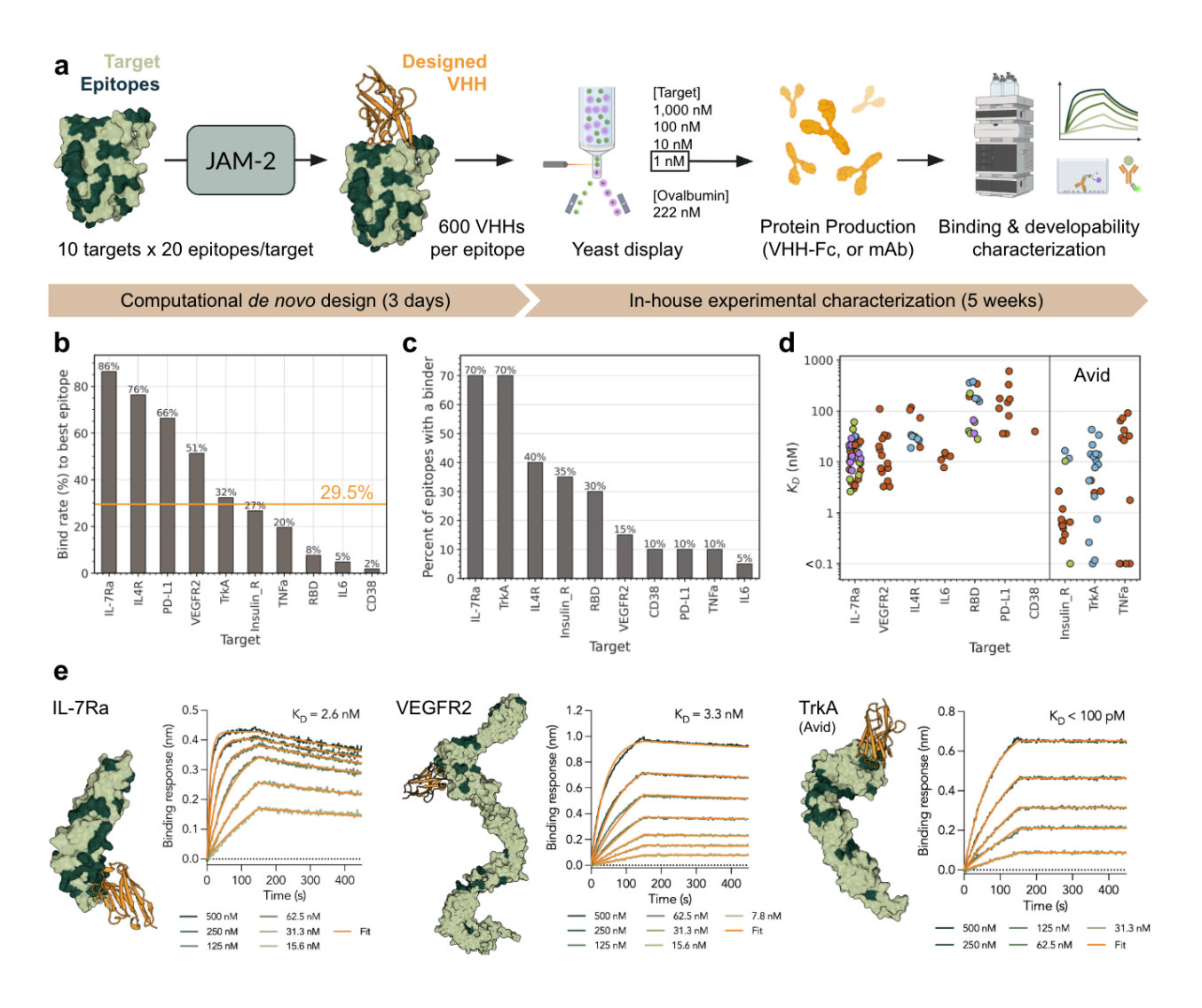


Figure 2: JAM-2 achieves state-of-the-art epitope breadth, successfully targeting user-specified epitopes. a. For each of 10 targets, 20 biophysically diverse epitopes were selected. Against each epitope, JAM-2 generated ~600 de novo VHH designs, which were screened by yeast surface display across a range of antigen concentrations. Designs that retained binding at 1 nM antigen were produced recombinantly (as VHH-Fc) and subjected to affinity and developability characterization. b. For each target, bind rate of the best-performing epitope. The orange line indicates the median bind rate across targets (~29.5%). c. Percent of designed epitopes per target (out of 20) that yielded at least one binder. d. Binding affinities of recombinant VHH-Fc antibodies across targets, measured by BLI. Binders for which an accurate K_D ($R^2 > 0.95$) was not calculable are excluded. The "Avid" group denotes designs whose binding is impacted by avidity effects that stem from natural antigen multimericity. e. Cherry-picked *de novo* designed antibodies and corresponding BLI sensorgrams for IL-7R α (left), VEGFR2 (middle), and TrkA (right).

JAM-2 reliably targets multiple, diverse epitopes

A major motivation for epitope-specific biologics design is functional diversity. When bound, different epitopes drive distinct mechanisms of action and signaling pathways. For many targets, the therapeutically relevant epitope is unknown and often missed with traditional immunization and display based approaches. Being able to intentionally bind multiple epitopes, rather than relying on chance, is essential. The strong hit rates and affinities in Target Set 1 suggested that JAM-2 could support systematic epitope-level exploration with high return on effort.

We evaluated epitope breadth on 10 targets, selecting 20 surface patches per antigen that spanned a wide range of physicochemical and structural properties (Fig. 2a, Table 1). These epitopes covered the full diversity of hydrophobicity, charge, polarity, and secondary structure present across each target's surface. To avoid prematurely filtering out designs for inherently difficult epitopes, we took the top 600 designs per epitope, yielding 12,000 VHHs. We call this set of targets Target Set 2.

Designs were screened by yeast display against each target at 1 μ M, 100 nM, 10 nM, and 1 nM antigen. Target-binding populations were isolated and sequenced (Supp. Fig. 3). To measure non-specific binding, we also collected binders to 222 nM ovalbumin, a known polyspecificity reagent (Fig. 2a). Designs were considered bona fide binders if they bound at 100 nM target and did not bind ovalbumin.

Across targets, designs to the most successful epitope bound with a median ~29.5% hit rate (Fig. 2b). Epitope-to-epitope variability was substantial: some epitopes supported high hit rates, whereas others were more challenging, yielding few to no binders (Supp. Fig. 4). Nevertheless, for half of the targets, JAM-2 produced binders to 30–70% of all selected epitopes – coverage that is difficult to access with traditional discovery, in which immunization and display often converge onto one or two dominant surface patches (Fig. 2c). Unsurprisingly, designs tended to bind epitopes with some hydrophobic character, and low polarity (Supp. Fig. 5).

Prioritizing epitope coverage, a subset of on-yeast binders showing binding at 1 nM target concentration were expressed as VHH-Fcs to determine binding affinities and in their therapeutically relevant recombinant form. For all 10 targets, we obtained single- to double-digit nanomolar affinities (Fig. 2d, Supp. Fig. 6).

Given JAM-2 designs are ranked, we could retrospectively evaluate bind rates and affinities of the top 45 designs that would only have been tested under a smaller testing budget. For 4 of 10 targets, we saw significantly higher bind rates (binding at 100 nM [target] on-yeast) ranging from 20-90%. For 6 of 10 targets, a confirmed single-digit nM binder was present in the top 45 ranked designs.

Cherry-picked structures for *de novo* designed VHH-Fc antibodies and corresponding BLI data are shown in Fig. 2e.

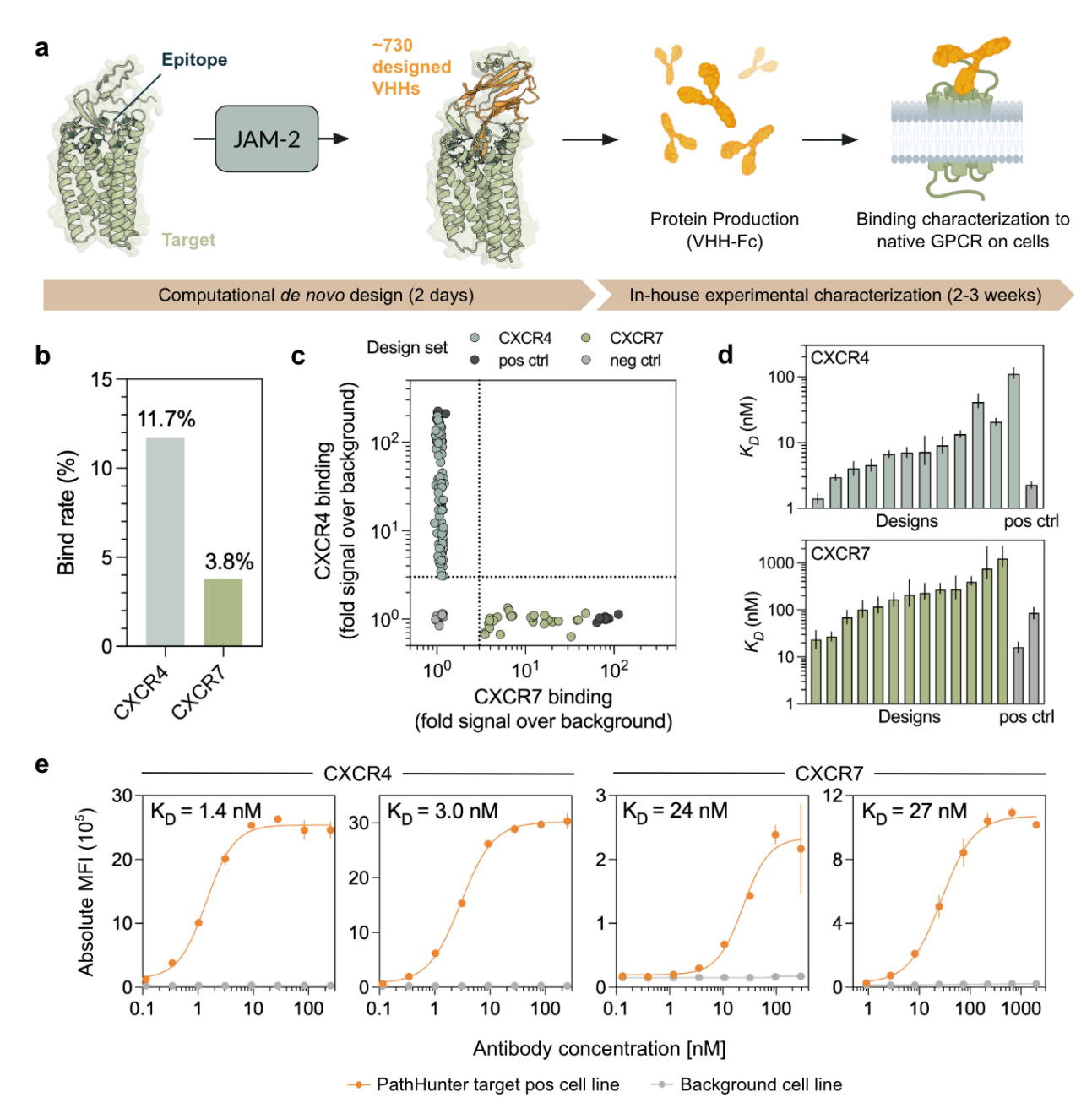


Figure 3: JAM-2 can target GPCRs with single- to double-digit success rates, and with drug-like affinities. a. For each GPCR target, JAM-2 generated ~730 *de novo* VHH designs which were expressed recombinantly as VHH-Fcs and screened for specific receptor binding on GPCR-overexpressing cell lines (PathHunter) and their matched parental (non-expressing) cell lines. b. On-cell bind rate in single-point binding assay for CXCR4 and CXCR7 antibodies evaluated at an average of 0.65 μM for CXCR4 and 1.09 μM for CXCR7. c. Single-point binding signal for CXCR4 and CXCR7 antibody designs measured against both CXCR4 and CXCR7 cell lines. d. On-cell K_D measurements from titrations of highest single-point MFI CXCR4 designs on the PathHunter CXCR4 cell line (top), and CXCR7 designs on the PathHunter CXCR7 cell line (bottom). Error bars are 95% CI. Respective benchmark antibodies are shown in grey. e. Binding curves of top CXCR4 designs (left) and CXCR7 designs (right) against their respective PathHunter target positive (orange) and matched background (grey) cell line.

JAM-2 targets GPCRs with single- to double-digit success rates, and generates low nanomolar binders to cryptic orthosteric epitopes

GPCRs remain among the most therapeutically important but technically difficult antibody targets^{15,16}. Their membrane-embedded architecture, conformational heterogeneity, and cryptic orthosteric epitopes have made them poorly compatible with traditional immunization and display, which struggle to present GPCRs in native conformations. While a handful of GPCR-directed antibodies have reached the clinic, these predominantly recognize extracellular loops or extended N-terminal domains¹⁷. Antibodies that engage GPCR orthosteric pockets remain elusive, despite these sites being critical determinants for therapeutic modulation.

To test whether JAM-2 could access these epitopes, we evaluated ~730 *de novo* designed VHHs targeting orthosteric pockets of each CXCR4 and CXCR7, two closely-related chemokine GPCRs activated by a shared ligand SDF1α (Supp. Fig. 7). No prior data on these targets were included in JAM-2 training. All designs were expressed individually as VHH-Fcs in ExpiCHO and tested directly on cell lines overexpressing each GPCR, alongside matched parental (non-expressing) cell lines, enabling concurrent measurement of bind-rate and receptor specificity for each design (Fig. 3a). No proxy screens or reagents (e.g., purified ECDs, engineered multimers) were used and all measurements were made directly against full-length receptors in their native membrane context (on-cell binding). Each experiment included benchmark VHHs discovered through traditional and laborious immunization and phage panning as positive controls (CXCR4: 238D2¹⁸; CXCR7: 07B11 and 08A10^{18,19}, all from Ablynx). We note that while immunization and phage panning previously worked for these targets, these approaches often fail for GPCRs as a broader target class.

Remarkably, JAM-2 achieved on-cell bind rates of 11.7% for CXCR4 (86/736 designs) and 3.8% for CXCR7 (28/728 designs) (Fig. 3b). Binders were defined as designs producing ≥3-fold higher signal on the GPCR-expressing cell line relative to the matched parental line in a single-point binding assay at an average antibody concentrations of 0.65 µM for CXCR4 and 1.09 µM for CXCR7 across binders (Fig. 3b, Supp. Fig. 8). Binding antibodies were highly target-specific and showed no undesirable cross-reactivity to the unintended GPCR indicating JAM-2 can discriminate between closely related epitopes (Fig. 3c).

A subset of 12-13 designs, prioritized by highest fold signal over background in the one-point screen, were titrated on cells to establish on-cell K_D values. From only ~730 designs, JAM-2 generated multiple single-digit nanomolar affinity antibodies to CXCR4, and multiple double-digit nanomolar affinity antibodies to CXCR7 (Fig. 3d, Supp. Fig. 9). Tightest antibodies evaluated showed on-cell KD values of 1.4 nM (CXCR4) and 23 nM (CXCR7), competitive with or surpassing their corresponding benchmark VHHs tested (Fig. 3e).

Taken together, these data show that a single JAM-2 design round can deliver multiple GPCR-selective antibodies with affinities comparable to or exceeding those obtained from traditional and far more laborious immunization and display campaigns. Importantly, JAM-2 high success rates enabled us to evaluate designs directly on native receptors and without any target-specific training data or iterative optimization. Importantly, *de novo* designed antibodies

directly accessed known functional epitopes in the orthosteric pockets, frequently inaccessible to traditional antibody discovery.

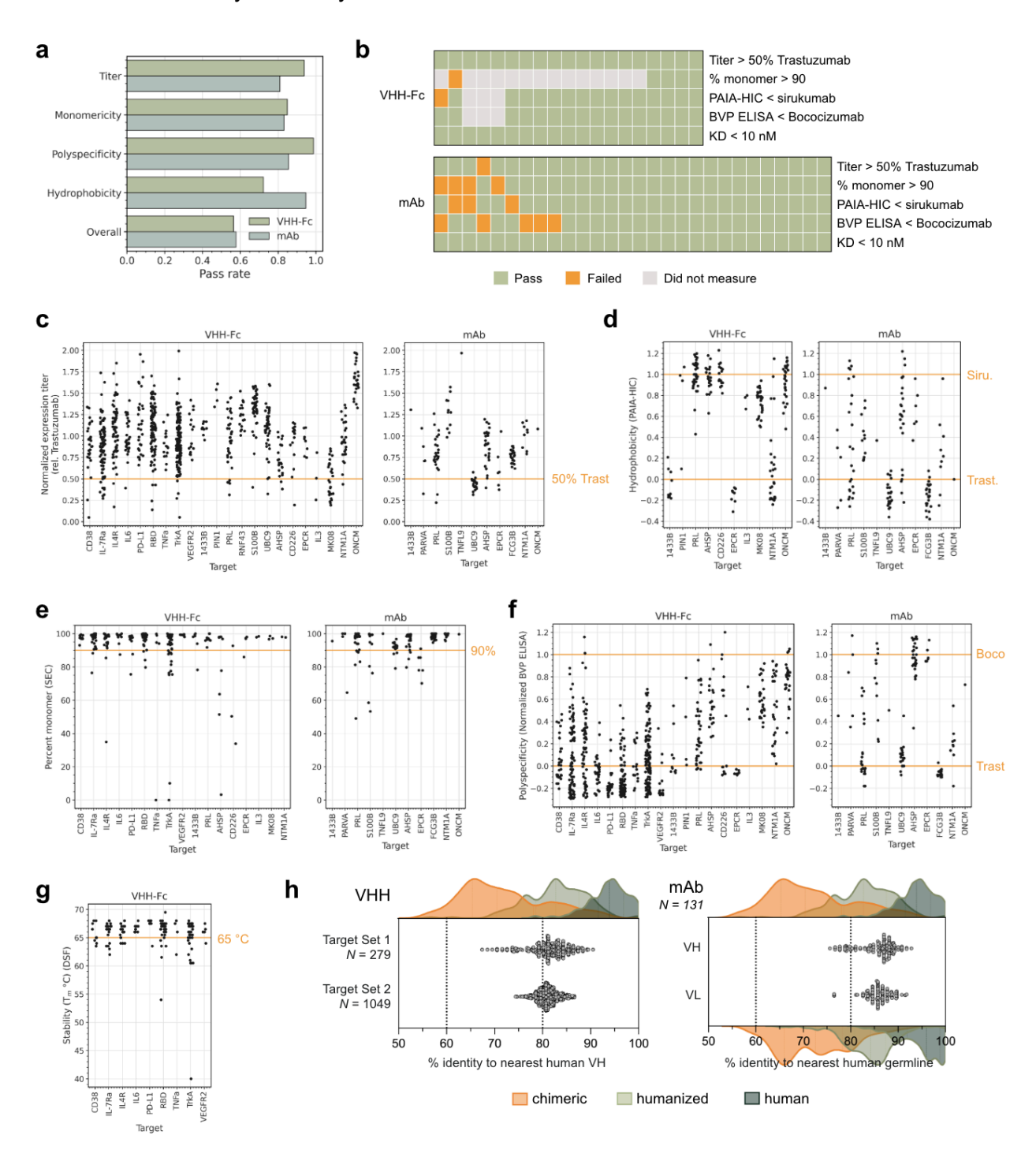


Figure 4: JAM-2 designs have strong developability profiles. a. Fraction of JAM-2–designed VHH-Fcs (green) and mAbs (blue) passing individual developability criteria (expression titer, monomericity, hydrophobicity, polyspecificity). Bottom bars show the overall pass-rate (all four properties passed). b. Per-antibody developability profiles for VHH-Fcs (top) and mAbs (bottom) for *de novo* designed binders with $K_D < 10$ nM and that were subject to any developability characterization. Each column is a single design and each row corresponds to a criterion (titer >50% of trastuzumab, monomericity >90%, PAIA-HIC signal below sirukumab, BVP

ELISA signal below bococizumab, K_D<10 nM). Green indicates pass, orange indicates fail, and grey indicates no measurement was made. **c-g**. Distributions of assay values for individual designs across targets (VHH-Fc, left; mAb, right where applicable). In all scatter plots, each point represents a single *de novo* designed antibody. Orange lines mark benchmark antibodies or pass thresholds. All available measurements are shown in the plots; missing points indicate designs for which sufficient material was not obtained or the assay was not performed. **c.** Expression titers in ExpiCHO, normalized to concurrently expressed trastuzumab. Pass rate is marked by a 50% trastuzumab threshold (higher is better). **d.** Hydrophobicity measured by PAIA-HIC. Benchmarks shown are sirukumab (upper line; high but acceptable hydrophobicity) and trastuzumab (lower line; low hydrophobicity) (lower is better). **e.** Monomericity percentage evaluated by SEC with a pass-rate of ≥90% monomer threshold after a single purification step without polishing (higher is better). **f.** Polyspecificity measured by BVP ELISA and normalized to control antibodies. Benchmarks include bococizumab (upper line; high polyspecificity) and trastuzumab (lower line; low polyspecificity) (lower is better). **g.** Thermostability of VHH-Fcs measured by DSF, reported as Tm, with 65 °C threshold used for a pass call (higher is better). **h.** Humanness of designs as the percent amino acid sequence identity to nearest human germline for VH or VH and VL sequences for VHH binders from Target Set 1 and Target Set 2 (left) and mAb binders from Target Set 1 (right). Colored kernel density estimates outside of the stripplot indicate % identity to nearest human germline values for clinical stage chimeric, humanized, and human antibodies deposited in Thera-SAbDab²⁰.

De novo designed antibodies show clinically relevant developability and are novel in sequence and structure

Developability is a central gatekeeper in biologics development. Key properties including expression, self-association, hydrophobicity, and polyspecificity collectively determine whether an antibody can be manufactured at scale, remain stable over a desirable shelf-life, and avoid off-target interactions that compromise antibody safety and efficacy to derail clinical programs. Across the industry, prior work has shown that these measurable biophysical dimensions are broadly predictive of both liabilities in later stage pre-clinical testing and even clinical success²¹.

To evaluate the developability of *de novo* designed antibodies across diverse targets, we characterized JAM-2-designed binders from Target Set 1 and Target Set 2 with respect to major biophysical properties used in early-stage antibody engineering²²: expression titer (N = 923), monomericity (N = 341), hydrophobicity (N = 311), polyspecificity (N = 821), and thermostability (N = 165). For each property, pass/fail criteria were determined using clinically-validated benchmarks or industry-accepted standards (Methods). When considering the four primary criteria – titer, monomericity, hydrophobicity, and polyspecificity – 57% of all designed antibodies passed all properties simultaneously (Fig. 4a). At the level of individual properties, pass rates were typically 80% or higher for both VHH-Fcs and mAbs. Importantly, single-digit nanomolar and picomolar binders showed strong developability profiles, with multiple designs passing all criteria (Fig. 4b). Excitingly, these designs – straight from the computer – may require no further optimization at all.

We note that JAM-2–designed GPCR binders were not included in this developability panel; however, *de novo* JAM-based GPCR antibodies have been characterized previously in a dedicated study¹³, and their developability profiles are expected to be broadly consistent with those observed here.

The raw distributions for each metric are shown in Figures 4c–g and Supp. Fig 10, with horizontal lines marking the relevant pass thresholds or benchmark antibody values. Most designs cluster within clinical-stage ranges, and developability performance is broadly consistent across targets and formats. Among the properties assessed, hydrophobicity shows the most pronounced target-dependent variation.

Humanness is an important developability attribute linked to reduced anti-drug antibody responses²³. JAM-2–generated VHHs and mAbs showed humanness levels comparable to clinical-stage humanized or fully human antibodies, supporting their suitability as therapeutic candidates (Fig. 4h).

Lastly, we assessed sequence and structural novelty for all double-digit-nanomolar or better binders from Target Sets 1 and 2. Nearly all designs (185/193) were >10% dissimilar to their nearest neighbor in a combined database of OAS (OPIG), INDI (NaturalAntibody), and NCBI NR (>3 billion sequences) (Supp. Fig. 11). Structural novelty was similarly high: >95% of designs had target-aligned RMSDs >10 Å relative to the closest antibody—antigen complex in SAbDab. These results held whether comparing full variable domains, CDRs, or (H)CDR3 alone (Supp. Fig. 11).

Discussion

Our results show that JAM-2 can reliably generate high-affinity, developable antibodies directly from design across a wide range of targets, without target-specific training data or iterative optimization. In a true zero-shot setting on 16 unseen, structurally diverse targets, JAM-2 produced binders to all of them using only 45 designs per format, routinely achieving drug-quality affinities and developability profiles comparable to those obtained through traditional display or immunization. Notably, many top designs exhibited lead-like profiles that may not require any further optimization at all.

JAM-2 is also the first system to demonstrate systematic epitope targeting. Across 10 antigens and 20 predefined epitopes each, the model generated binders to 30–70% of user-specified epitopes for half the targets. This breadth turns what is normally an emergent, stochastic outcome of an immunization or display campaign into a controllable design parameter, enabling purpose-built panels that tile functional regions, dissect mechanisms, or intentionally avoid immunodominant surfaces.

GPCRs illustrate the value of this precision. These receptors have historically resisted antibody discovery, especially at their orthosteric pockets—sites central to function but structurally cryptic and poorly presented in most screening formats. JAM-2 generated direct on-cell binders to CXCR4 and CXCR7 with hit rates up to 11%, and top designs in the single-digit nanomolar range, all against full-length receptors in their native membrane context and without proxy antigens or avidity-enhancing scaffolds. This demonstrates that a single cycle of *de novo* design — with no intermediate wet-lab work — can now produce binders suitable for immediate functional testing in therapeutically relevant cellular assays, even for tough targets.

While JAM-2 was evaluated here primarily as a generator of therapeutic-grade binders — emphasizing affinity, specificity, hit-rates, and developability — we did not systematically classify mechanisms of action. For GPCRs, for example, we showed nanomolar binding to orthosteric pockets on cells but did not distinguish agonism, antagonism, or signaling bias, nor map how epitope choice relates to functional outcomes. Extending JAM-2 to triage or design directly for

specific mechanisms of action is a natural next step, and would enable design-driven campaigns that progress smoothly into more advanced functional and in vivo models. JAM-2 now serves as a foundation for the next stage of *de novo* design. The ability to reliably target specific epitopes opens access to regions historically inaccessible to antibody discovery, including GPCR orthosteric sites, quaternary interfaces, post-translational modifications, and other poorly immunogenic or structurally recessed features. Intentional control over geometry of engagement will support the design of antibodies with defined functional outcomes such as antagonism, agonism, biased signaling, or internalization.

Equally important, computational design enables *parallel* discovery across many targets, dramatically reducing experimental load and accelerating early-stage hypothesis testing. In our hands, for Target Set 1 alone, 16 independent discovery campaigns across two antibody formats progressed from initial design to purified affinity measurements in under four weeks, executed by just a four-person experimental team.

Finally, the high hit rates afforded by JAM-2 now allows antibodies to be generated in a push-button fashion and tested directly in the most human-relevant contexts available, late-stage cellular assays, ex vivo systems, and even animal models. By reducing reliance on early, artificial screening proxies, this approach may improve translational fidelity and help address one of the central challenges in drug development: the high failure rate that stems from over-optimization for early discovery assays rather than human-relevance.

Experimental Methods

De novo designed yeast surface display library construction

To construct the yeast surface display libraries, oligonucleotides encoding the designed VHH antibodies were ordered from Twist Biosciences as 300nt oligo pools with flanking Bsal recognition sites for Golden Gate assembly. All DNA was codon-optimized for expression in *S. cerevisiae*. Golden gate assembly reactions were run overnight using PCR amplified oligo pool DNA to clone into the yeast display vector, pCTcon2.

Purified golden gate reactions were electroporated into NEB 10-beta electrocompetent *E. coli* (New England Biolabs) using the pre-set bacterial protocol on the Gene Pulser Xcell Electroporation System (BioRad). Serial dilutions of the bacterial transformants were plated and verified to represent a greater than 100-fold coverage of the library. The resulting plasmid library was extracted from the bacterial cultures using a QIAprep Spin Miniprep kit (QIAGEN).

The assembled libraries were linearized and transformed into *S. cerevisiae* strain EBY100 (ATCC) using a standard lithium acetate and DTT-based yeast electroporation protocol as described by Van Deventer et al.²⁴ Transformants were serial diluted and plated post recovery to verify library coverage was at least 100-fold. Yeast transformants were cultivated in synthetic dextrose medium with casamino acids (SDCAA) pH 4.5 (Teknova) shaking at 30°C overnight.

Cell sorting of yeast surface displayed antibody libraries

Yeast libraries were grown to saturation overnight in SDCAA pH 4.5 media (Teknova) shaking at 30°C. Each library was passaged into fresh SDCAA pH 4.5 media at a 25X dilution and grown for 2-4 hours before pelleting via centrifugation at 2000 x g for 5 minutes. To induce the libraries, cell pellets were resuspended to a OD600 of 1 in synthetic galactose medium with casamino acids (SGCAA) (Teknova) and incubated at 20°C for 20 hours.

Fluorescence-Activated Cell Sorting (FACS):

For sorting, induced yeast cells were washed twice with 1% PBSA (1% BSA in 1X PBS). The libraries were incubated with anti-c-Myc-AF488 antibody (1:100x dilution, 16-308, Sigma-Aldrich) to label yeast cells displaying full length VHHs, and the desired antigen concentrations to evaluate antigen binding for 1 hour at room temperature. The samples were spun down at 4°C and washed twice with ice-cold 1% PBSA to remove unbound antigen and c-Myc antibody. 1:100X dilution of the relevant secondary antibody (Table 1) was added and the samples were incubated on ice for 30 minutes. The samples were spun down at 4°C and washed twice with ice-cold 1% PBSA to remove any excess secondary antibody.

Table 1: Target Set 2 Antigens: Yeast surface display library enrichment and reagent information.

Target ID	Antigen Description	Valency	First enrichment	Second enrichment	Secondary antibody
--------------	---------------------	---------	------------------	-------------------	-----------------------

IL4Ra	Human IL-4 R alpha / CD124 Protein, His Tag (MALS verified) (Acro Biosystems; ILR-H5221)	Monovalent	1000 nM	1 nM 10 nM 100 nM 1000 nM	anti-His Tag-AF647 (IC0501R; R&D Systems)
TNFa	Human TNF-alpha Protein, His Tag, active trimer (MALS verified) (Acro Biosystems; TNA-H5228)	Trivalent	1000 nM	1 nM 10 nM 100 nM 1000 nM	anti-His Tag-AF647 (IC0501R; R&D Systems)
IL6	Human IL-6 Protein, His Tag (MALS verified) (Acro Biosystems; IL6-H5243)	Monovalent	1000 nM	1 nM 10 nM 100 nM 1000 nM	anti-His Tag-AF647 (IC0501R; R&D Systems)
VEGFR2	Human VEGF R2 / KDR Protein, His Tag (MALS verified) (Acro Biosystems; KDR-H5227)	Monovalent	1000 nM	1 nM 10 nM 100 nM 1000 nM	anti-His Tag-AF647 (IC0501R; R&D Systems)
CD38	Human CD38 Protein, His Tag (MALS verified) (Acro Biosystems; CD8-H5224)	Monovalent	1000 nM	1 nM 10 nM 100 nM 1000 nM	anti-His Tag-AF647 (IC0501R; R&D Systems)
Insulin_R	Human Insulin R / CD220 (28-944) Protein, His Tag (MALS & SPR verified) (Acro Biosystems; INR-H52Ha)	Bivalent	1000 nM	1 nM 10 nM 100 nM 1000 nM	anti-His Tag-AF647 (IC0501R; R&D Systems)
TrkA	Human TrkA / NTRK1 (33-417) Protein, Mouse IgG2a Fc Tag (Acro Biosystems; TRA-H5259)	Bivalent	1000 nM	1 nM 10 nM 100 nM 1000 nM	Anti-mouse IgG2a Fc-AF647 (407116; BioLegend)
IL-7Ra	Human IL-7 R alpha / CD127 Protein, His Tag (Acro Biosystems; IL7-H52H7)	Monovalent	1000 nM	1 nM 10 nM 100 nM 1000 nM	anti-His Tag-AF647 (IC0501R; R&D Systems)
RBD	SARS-CoV-2 (COVID-19) S protein RBD, His Tag (MALS verified) (Acro Biosystems; SPD-C52H3)	Monovalent	1000 nM	1 nM 10 nM 100 nM 1000 nM	anti-His Tag-AF647 (IC0501R; R&D Systems)
PD-L1	Human PD-L1 / B7-H1 Protein, His Tag (MALS verified) (Acro Biosystems; PD1-H5229)	Monovalent	1000 nM	1 nM 10 nM 100 nM	anti-His Tag-AF647

Samples were sorted on a Sony SH800 cell sorter using normal or ultra purity mode depending on the stage of enrichment. Sorted binders were collected in SDCAA pH 4.5 media and shaken at 30°C for 2-3 days until saturated.

Next generation sequencing of sorted yeast surface display populations

Binders isolated from the second enrichment were yeast miniprepped using a Zymoprep Yeast Plasmid Miniprep II kit (Zymo Research). DNA was then electroporated into NEB 10-beta electrocompetent *E. coli* (New England Biolabs) and recovered in LB liquid medium supplemented with carbenicillin. *E. coli* cultures were miniprepped using a QIAprep Spin Miniprep kit (QIAGEN) and then submitted for sequencing using Oxford Nanopore technology.

For YSD data, nanopore reads were mapped to the coding DNA of JAM-2-generated designs, and the number of reads that aligned to each design are tabulated. Due to sequencing noise, some designs have non-zero but low read count levels, whereas designs truly present in the binding population have higher read counts. To classify binders from non-binders, we set a read count threshold based on the empirical cumulative distribution function (eCDF) of read counts in the sample. Typically, 80-90% of reads are accounted for by a small number of designs, and the presence of clear "elbow" in the eCDF suggests a natural read count threshold that separates non-binders from binders. Empirically, we have validated this strategy identifies binding designs such that when expressed recombinantly and tested individually, designs are highly likely to bind the target.

Mammalian protein production

Designs for recombinant protein production were synthesized either as oligo pools (Twist Biosciences) for random colony picking or as individual gene fragments (Twist Biosciences). All constructs were codon-optimized for expression in *Homo sapiens* and cloned into pcDNA3.4 (Invitrogen) using Golden Gate cloning as described previously¹². All in-house produced antibodies and Fc-tagged proteins are of human IgG1 antibody subclass and contain the L234A, L235A, P329G (LALA PG) mutations to reduce effector function²⁵. VHH-Fcs were produced in a VHH-G4S-Fc format.

For GPCR designs, an oligo pool with thousands of unique designs was utilized. Briefly, purified golden gate reactions were electroporated into NEB 10-beta electrocompetent *E. coli* (New England Biolabs) using the pre-set bacterial protocol on the Gene Pulser Xcell Electroporation System (BioRad). Dilutions of the bacterial transformants were plated on LB agar plates containing carbenicillin for random colony picking of about 730 clones.

Colonies were inoculated into 96 deep well blocks containing Terrific Broth (TB) media supplemented with carbenicillin and grown overnight until saturation. Pelleted cultures were

then miniprepped to obtain transfection-grade plasmid. Upon identification of hits, sequences were verified by NGS.

For protein production, plasmids were transiently transfected into ExpiCHO cells (1 μ g DNA/ mL cell culture) using the ExpiCHO Expression System (Gibco). Following harvest 6 days after transfection, the cell culture supernatant was clarified by centrifugation at 2000-3000 x g for 20-30 minutes. Concentrated (10X) phosphate buffered saline (PBS), pH 7.4 was added to the supernatant to achieve a final concentration of 1X PBS.

Quantification of antibody titers

Antibody titer was quantified using BLI. The clarified supernatant was diluted 5-fold in Octet Buffer (composed of 1X PBS, 0.1% BSA, and 0.05% TWEEN20). Octet ProteinA biosensors (Sartorius) were hydrated in supernatant from an empty vector transfection 5-fold diluted in Octet buffer and equilibrated alongside the sample plate at 30°C for 10 minutes prior to the start of the experiment. Biosensors were shaken at 1000 rpm for 60 seconds in the samples. A standard curve was created using known concentrations of VHH-Fc or mAbs diluted in mammalian supernatant and Octet buffer at a 1:4 dilution. Sample binding rate over the first 60 seconds of association to the biosensor was measured. Octet Analysis Studio 13.0.2.46 software was used to build the standard curve and apply it for quantitation of samples. Expression titers are normalized to an in-plate and concurrently produced Trastuzumab control. For a passable expression titer, designs were required to reach at least 50% of the ExpiCHO titer of Trastuzumab, a clinically validated, highly developable benchmark.

Protein purification

Fc-containing proteins were purified using either rProtein A Sepharose Fast Flow antibody purification resin (Cytiva), Pierce™ Protein A/G Magnetic Agarose Beads (Thermo Scientific), or Mag Sepharose™ PrismA magnetic bead resin (Cytiva). The resin/beads were equilibrated in 1X PBS then added to the ExpiCHO supernatant and mixed for 30 minutes to achieve binding. Two washes with 1X PBS were performed to remove residual supernatant and non-specific proteins, followed by two brief washes with water to remove residual PBS. Bound proteins were then eluted with IgG Elution Buffer, pH 2.8 (Thermo Scientific), then neutralized with 1 M Tris-HCI (Invitrogen) to approximately pH 7.

Following purification, the eluted protein solutions were buffer exchanged into PBS using Zeba™ Spin Desalting Columns or Plates (Thermo Scientific). The final protein concentration was quantified via A280.

Monomericity - Size Exclusion Chromatography

Proteins were analyzed using an Agilent 1100 system equipped with either an SRT C SEC 300 column (235300-7830; Sepax Technologies) or an AdvanceBio SEC 300Å column (PL1180-3301; Agilent), following a one-step Protein A purification. Affinity-purified samples were desalted into 1X PBS (pH 7.4) and diluted to 0.25 mg/mL. For SEC, 6.25 µg of protein was injected using an autosampler and eluted at 1 mL/min using 150 mM sodium phosphate and 20 mM imidazole (pH 7.0) as the mobile phase. Chromatograms were analyzed with ChemStation

software to determine percent monomer content. Passing monomericity thresholds were set at >90% monomer after a single purification step without polishing.

Hydrophobicity and Ovalbumin Polyreactivity Assays

Hydrophobicity and ovalbumin binding were measured using PAIA Biotech developability kits (PA-DEV-HIC and PA-DEV-OVA; PAIA Biotech). Each assay used its corresponding 384-well PAIA plate. Samples were adjusted to 2 μ M in 1x PBS and diluted to 67 nM in deionized water. 40 μ L of PAIA reagent and 20 μ L of sample were dispensed in duplicate into each well of the respective 384-well PAIA plate. Plates were shaken at 2200 rpm for 30 minutes, followed by 1500 rpm for 10 minutes, centrifuged briefly at 1500 x g, and fluorescence was read on an iD3 SpectraMax Microplate Reader (Molecular Devices) plate reader in bottom read mode at 630/670 nm. Data is presented as the average of two replicate wells. For PAIA assays, the results were normalized from 0 to 1, where 0 is the value associated with a low scoring control antibody (Trastuzumab for low hydrophobicity and ovalbumin binding) and 1 is the value associated with a high scoring control antibody (Bococizumab for high ovalbumin binding and Sirukumab for high hydrophobicity).

Polyspecificity - Baculovirus Particle (BVP) ELISA

BVP ELISA was performed as described in Jain et al. 22 25 µL of 1% baculovirus particles in PBS (MEDNA Scientific) were diluted with equal volume of 50 mM sodium carbonate (pH 9.6) per well, and incubated on high bind ELISA plates (3369; Corning) at 4°C overnight with shaking. The next day, unbound BVPs were removed from the wells and the plate was washed 3x with 100 µL of 1X PBS. All remaining steps were performed at room temperature. 100 µL of blocking buffer (PBS with 0.5% BSA) was added to the plate and incubated for 1 hour at room temperature with shaking at 450 rpm. Following incubation, the plate was washed 3x with 100 µL of 1X PBS. Next, antibodies were diluted to 1 µM in blocking buffer and wells were treated with 50 µL for 1 hour at room temperature with shaking at 450 rpm. The plate was then washed 6x with 100 µL of 1X PBS. 50 µL of 100 ng/mL secondary anti-Fc-HRP conjugate (Thermo A18817) was added to the wells and incubated for 1 hour at room temperature. The plate was then washed 6x with 100 µL of 1X PBS. Finally, 50 µL of room temperature TMB substrate (34028; Thermo Scientific) was added to each well and incubated for ~1-2 minutes with gentle shaking. The reactions were stopped by addition of 50 µL 4N sulfuric acid to each well.

Absorbance at 450 nm was read on an iD3 SpectraMax Microplate Reader (Molecular Devices). BVP scores were determined by normalizing raw absorbance to control wells with no test antibody (i.e. BVP-only control). Data is presented as the average of two replicate wells. The results were normalized from 0 to 1, where 0 is the value associated with a low BVP binding control antibody (Trastuzumab) and 1 is the value associated with a high BVP binding control antibody (Bococizumab).

Protein Stability - Differential Scanning Fluorimetry (DSF)

The melting temperature or thermal stability of purified proteins was determined using DSF with the GloMelt Thermal Shift Protein Stability Kit (Biotium). The protocol provided by the

manufacturer was followed, briefly: A 10X GloMelt dye working stock was freshly prepared from the 200X stock using PBS to dilute. Next, proteins were prepared and diluted such that the final in assay concentration was 0.5 μ g/ μ L. Each reaction was prepared to contain a final concentration of 1X dye, 0.5 μ g/ μ L protein, and PBS in a total volume of 20 μ L. Reactions were prepared in qPCR plates with an optical seal. The melt curves were collected using a Bio-Rad CFX Opus 96 real-time PCR thermocycler and signal was detected in the SYBR channel. The protocol steps were as follows: 1) 25°C for 3 min, 2) 25-95°C ramp at a rate of 0.5°C per 5 seconds, 3) 95°C for 3 min. The negative melt curve derivative results were plotted and the temperature associated with the peak of the curve was assigned as the melting temperature. A passing melting temperature threshold of 65 °C was set.

Bind-rate evaluation - Biolayer Interferometry

A RH96 Octet system with 384-Well Tilted-Bottom Microplates (Sartorius) was used to analyze binary binding of Target Set 1 antigens. His-tagged antigens listed in Table 2 were immobilized on Octet HIS1K biosensors (Sartorius) biosensors with bivalent binders (VHH-Fc or mAb) assessed directly in ExpiCHO supernatant (pre-purification) as the analyte. Briefly, biosensors were hydrated in an Octet buffer composed of 1X PBS, 0.1% BSA, and 0.05% TWEEN20, and equilibrated alongside the sample plate at 30°C for 10 minutes prior to start of the experiment. Octet HIS1K biosensors (Sartorius) were equilibrated in Octet buffer for 60 seconds prior to loading with 50 nM antigen (diluted in Octet buffer) with a target loading density of 0.5 nm.

The biosensors were then baselined in ExpiCHO supernatant for 60 seconds before initiating the association phase. During this phase, the biosensors were exposed to 500 nM VHH-Fc or mAb (diluted in ExpiCHO supernatant) for 300 seconds. Following the association phase, a 300-second dissociation phase in ExpiCHO supernatant was assessed. A reference sample containing negative control ExpiCHO supernatant (without antibody expressed) was also included and used for data correction.

His1K biosensors were regenerated for use up to 6 times. Before each measurement, biosensors were incubated at 1000 rpm for 5 seconds in regeneration buffer (10 mM glycine pH 1.0-1.5) followed by incubation at 1000 rpm for 5 seconds in neutralization buffer (Octet buffer). This regeneration cycle was repeated 3 times before biosensors were used for a measurement.

Hits were classified as antibody designs with >0.1 nm binding response to their target antigen after reference sample correction. For developability characterization, hits were then purified according to the methods described above. Up to 10 hits per format, per target, were selected based on single point binding data to evaluate binding affinities (see K_D evaluation methods section).

Table 2. Target Set 1 Antigens: reagent information.

Target ID	Antigen Description	Vendor and Catalog Number	Valency
AHSP	Human AHSP / EDRF Protein (Recombinant His, N-Terminal) (aa1-102)	LSBio; LS-G12132-10	Monovalent

CD226	Recombinant Human DNAM-1/CD226 Protein (ECD, His Tag), HPLC-verified	Sino Biological; 10565-H08H	Monovalent
EPCR	Recombinant Human EPCR Protein (His Tag), HPLC verified	Sino Biological; 13320-H08H	Monovalent
FCG3B	Recombinant Human CD16b/FCGR3B/Fc gamma RIIIB Protein (NA2 allotype, His Tag), HPLC-verified	Sino Biological; 11046-H08H	Monovalent
IL3	Recombinant Human IL-3 Protein (His Tag)	Sino Biological; 11858-H08H	Monovalent
MK08	Recombinant Human JNK1 His Protein	Novus Biologicals; NBP2-52123	Monovalent
PARVA	PARVA/alpha-Parvin Protein, Human (His)	MedChemExpress; HY-P7493	Monovalent
PIN1	Recombinant Human Pin1 Protein (His Tag)	Sino Biological; 10282-H07E	Monovalent
RNF43	Recombinant Human RNF43 Protein (His Tag), HPLC-verified	Sino Biological; 16108-H08H	Monovalent
TNFL9	Recombinant Human 4-1BB Ligand/TNFSF9 Protein (His Tag), Trimer, MALS-verified	Sino Biological; 15693-H07H2	Trivalent
UBC9	Recombinant Human UBC9/UBE2I Protein (Full Length, His Tag), Active	Sino Biological; U224-380H	Monovalent
NTM1A	METTL11A Protein, Human (His)	MedChemExpress; HY-P700638	Monovalent
1433B	Recombinant Human 14-3-3 beta Protein (Full Length, His Tag)	Sino Biological; Y71-30H	Bivalent
ONCM	Recombinant Mouse Oncostatin M/OSM Protein (His Tag)	Sino Biological; 50112-M08H	Monovalent
PRL	Recombinant Human Prolactin Protein (His Tag)	Sino Biological; 10275-H08B	Monovalent
S100B	Recombinant Human S100B Protein (His Tag), HPLC-verified	Sino Biological; 10181-H07E	Bivalent

K_D evaluation - Biolayer Interferometry

A RH96 Octet system with 384-Well Tilted-Bottom Microplates (Sartorius) was used to analyze binding. To avoid avidity effects in K_{D} determination, 1:1 interactions were assessed by immobilizing Fc-tagged (bivalent) antibodies (VHH-Fc or mAb) on the biosensors and using monovalent (His-tagged) antigens as the analyte, when possible. If monovalent antigen was not available or antigen natively multimerizes, reported kDs are avidity measurements and are reported as such in the text. Recombinant antigen information and their valencies are listed in Table 1 and Table 2. Briefly, Octet AHC2 biosensors (Sartorius) were hydrated in Octet buffer

composed of 1X PBS, 0.1% BSA, and 0.05% TWEEN20, and equilibrated alongside the sample plate at 30°C for 10 minutes prior to start of the experiment. Octet AHC2 biosensors (Sartorius) were equilibrated in the Octet buffer for 60 seconds prior to loading with 50 nM antibody in Octet buffer with a target loading density of 1 nm for VHH-Fcs and mAbs.

The biosensors were then baselined in Octet buffer for 60 seconds before initiating the association phase. During this phase, the biosensors were exposed to 7 antigen concentrations ranging from 7.8 nM to 500 nM in Octet buffer for 150 seconds. Antigens are listed in Table 1 and Table 2. Following the association phase, a 300-second dissociation phase in the Octet buffer was assessed. Dissociation phase was extended to 1200 s as necessary for some antibodies with minimal dissociation. A reference sample containing only the Octet buffer instead of antigen was included for each antibody and a reference sensor (without antibody loaded) was included for each antigen concentration and used for data correction.

AHC2 biosensors were regenerated for use up to 6 times. Before each measurement, biosensors were incubated at 1000 rpm for 5 s in regeneration buffer (10 mM glycine pH 1.0-1.5) followed by incubation at 1000 rpm for 5 s in neutralization buffer (Octet buffer). This regeneration cycle was repeated 3 times before biosensors were used for a measurement.

The Octet Analysis Studio 13.0.3.52 software was used for K_D determination. For each design, concentrations above or below the optimal fitting range were excluded. At least 3 appropriate concentrations were chosen to fit each binder. For all targets, a 1:1 model global fit of the association and dissociation was used to determine K_D .

Kinetic data is presented for fits with full R^2 values greater than 0.95. For antigens where we did not identify binders that passed this threshold (ONCM), fits with full R^2 values greater than 0.90 and passing visual inspection are presented. Sensorgrams for all binders with full R^2 values greater than 0.90 are presented in the Supplementary Information (Supp. Fig 2 and Supp. Fig 6) for each target.

Using these analysis parameters, binders for which an accurate K_D was not calculable (full R^2 less than 0.90) under the conditions tested are excluded. "Avid" denotes designs whose binding is impacted by avidity effects that stem from antigen valency. For select sub-nanomolar binders, we were not able to measure adequate dissociation under the conditions tested – these cases are denoted in the text with K_D estimates.

K_D evaluation - Biolayer Interferometry

CHO-K1 (ATCC), PathHunter CHO-K1 CXCR7 β -arrestin (DiscoverX), C2C12 (ATCC), and PathHunter C2C12 CXCR4 β -arrestin (DiscoverX) cell lines were cultured under manufacturer recommended conditions. For flow cytometry binding assays, cells were harvested, uniquely labeled with CellTrace CSFE and Violet dyes (ThermoFisher Scientific), and pooled in equal ratios.

 $0.1x10^6$ pooled cells per well were directly treated with 50 µL clarified supernatant containing antibody for 2 hours at 4°C. After incubation, cells were washed four times with cold 1% PBSA, then stained with anti-Human Fc-647 secondary antibody (Biolegend) for 30 minutes at 4°C, and analyzed using a Novocyte Advanteon flow cytometer (Agilent). MFI signal was compared to the respective background cell line and designs yielding MFI values greater than 3-fold over background were classified as binders.

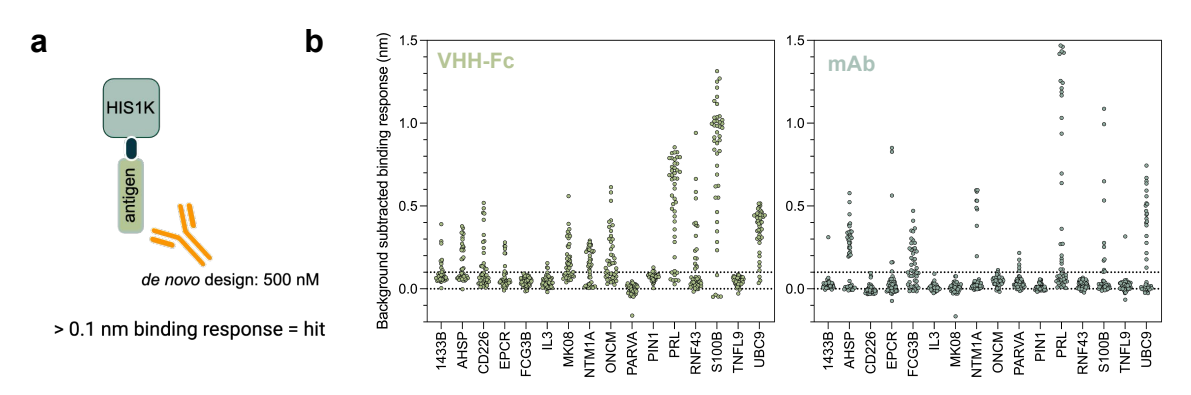
 $0.1x10^6$ pooled cells were treated with 8-point binder dilution series in 50 µL of clarified supernatant and incubated at 4°C for 2 hours. After incubation, cells were washed four times with cold 1% PBSA, then stained with anti-human Fc-647 secondary antibody (BioLegend) for 30 min at 4°C, and analyzed using a Novocyte Advanteon flow cytometer (Agilent). The MFI from the respective background cell line was subtracted, and EC50s (on-cell K_Ds) were calculated using a variable slope model in GraphPad Prism 10. EC50s with confidence intervals within one order of magnitude are presented.

References

- 1. Chan, A. C., Martyn, G. D. & Carter, P. J. Fifty years of monoclonals: the past, present and future of antibody therapeutics. *Nature Reviews Immunology* **25**, 745–765 (2025).
- Kothari, M. et al. A Comprehensive Review of Monoclonal Antibodies in Modern Medicine: Tracing the Evolution of a Revolutionary Therapeutic Approach. Cureus 16, e61983 (2024).
- 3. Crescioli, S. *et al.* Antibodies to watch in 2025. *mAbs* (2024) doi:10.1080/19420862.2024.2443538.
- 4. Jo, M. & Jung, S. T. Engineering therapeutic antibodies targeting G-protein–coupled receptors. *Experimental & Molecular Medicine* **48**, e207–e207 (2016).
- 5. Wilson, P. C. & Andrews, S. F. Tools to therapeutically harness the human antibody response. *Nature Reviews Immunology* **12**, 709–719 (2012).
- 6. Han, K. H., Li, Y.-C., Parveen, R., Venkataraman, S. & Lin, C.-W. Technologies for Monoclonal Antibody Discovery and Development. *Int J Mol Sci* **26**, (2025).
- 7. Bennett, N. R. *et al.* Atomically accurate de novo design of antibodies with RFdiffusion. *Nature* 1–11 (2025).
- 8. Chai-2. Zero-shot antibody design in a 24-well plate | bioRxiv doi:10.1101/2025.07.05.663018.
- 9. Germinal: Efficient generation of epitope-targeted de novo antibodies with Germinal | bioRxiv.
- 10. mBER: Controllable de novo antibody design with million-scale experimental screening | bioRxiv.
- 11. BoltzGen: Toward universal binder design.
- 12. Bio, N. & Biswas, S. De novo design of epitope-specific antibodies against soluble and multipass membrane proteins with high specificity, developability, and function. *bioRxiv* 2025.01.21.633066 (2025) doi:10.1101/2025.01.21.633066.
- 13. Website. De novo design of hundreds of functional GPCR-targeting antibodies enabled by scaling test-time compute | bioRxiv.
- 14. Dondelinger, M. *et al.* Understanding the Significance and Implications of Antibody Numbering and Antigen-Binding Surface/Residue Definition. *Front. Immunol.* **9**, 412684 (2018).
- 15. Lorente, J. S. *et al.* GPCR drug discovery: new agents, targets and indications. *Nature Reviews Drug Discovery* **24**, 458–479 (2025).
- 16. Hutchings, C. J., Koglin, M., Olson, W. C. & Marshall, F. H. Opportunities for therapeutic

- antibodies directed at G-protein-coupled receptors. *Nature Reviews Drug Discovery* **16**, 787–810 (2017).
- 17. Peterson, S. M. *et al.* Discovery and design of G protein-coupled receptor targeting antibodies. *Expert Opinion on Drug Discovery* 417–428 (2023).
- 18. Jähnichen, S. et al. CXCR4 nanobodies (VHH-based single variable domains) potently inhibit chemotaxis and HIV-1 replication and mobilize stem cells. *Proceedings of the National Academy of Sciences of the United States of America* **107**, 20565 (2010).
- 19. Descamps, F. *et al.* Bispecific anti-cxcr7 immunoglobulin single variable domains. *World Patent* (2012).
- 20. Raybould, M. I. J. *et al.* Thera-SAbDab: the Therapeutic Structural Antibody Database. *Nucleic acids research* **48**, (2020).
- 21. Jain, T. *et al.* Assessment and incorporation of in vitro correlates to pharmacokinetic outcomes in antibody developability workflows. *mAbs* (2024) doi:10.1080/19420862.2024.2384104.
- 22. Jain, T. *et al.* Biophysical properties of the clinical-stage antibody landscape. *Proceedings of the National Academy of Sciences* **114**, 944–949 (2017).
- 23. Martin, K. P., Grimaldi, C., Grempler, R., Hansel, S. & Kumar, S. Trends in industrialization of biotherapeutics: a survey of product characteristics of 89 antibody-based biotherapeutics. *mAbs* **15**, 2191301 (2023).
- 24. Van Deventer, J. A. & Wittrup, K. D. Yeast surface display for antibody isolation: library construction, library screening, and affinity maturation. *Methods Mol Biol* **1131**, 151–181 (2014).
- 25. Schlothauer, T. *et al.* Novel human IgG1 and IgG4 Fc-engineered antibodies with completely abolished immune effector functions. *Protein Eng Des Sel* **29**, 457–466 (2016).

Supp. Fig. 1. Bind-rate evaluation by BLI using a single-point assay. **a.** Diagram of BLI experimental set up used for hit determination. **b.** Binding response at 500 nM assessed in ExpiCHO supernatant



Supp. Fig. 2. a. Supp. Fig. 3. a. Diagram of BLI experimental set up used for K_D determination. **b.** BLI kinetic sensograms for JAM-2–designed antibodies binding 10 different antigens from Target Set 1. For each antigen, background-subtracted binding responses are shown for individual VHH-Fc or mAb designs; each panel corresponds to one antibody. Colored curves represent sensorgrams at a series of analyte concentrations (typically 7.8–500 nM), and red curves show global 1:1 Langmuir fits used to determine the apparent K_D , reported above each panel. The y-axis indicates background-subtracted binding response (nm) and the x-axis indicates time (s); vertical dashed lines mark transitions between baseline, association, and dissociation phases. Unless otherwise annotated in red, fits have $R^2 \ge 0.95$. Panels labeled "No confident k_{dis} " or with red R^2 values denote interactions where extremely slow dissociation or lower fit quality prevented a reliable kinetic K_D estimate.

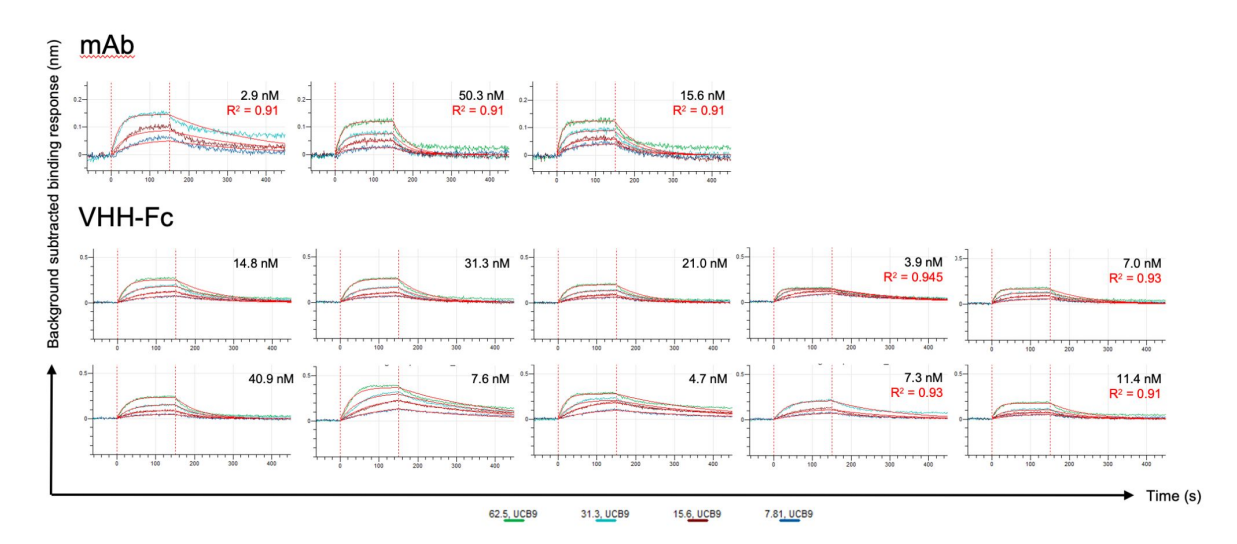
а



1:1 global fitting

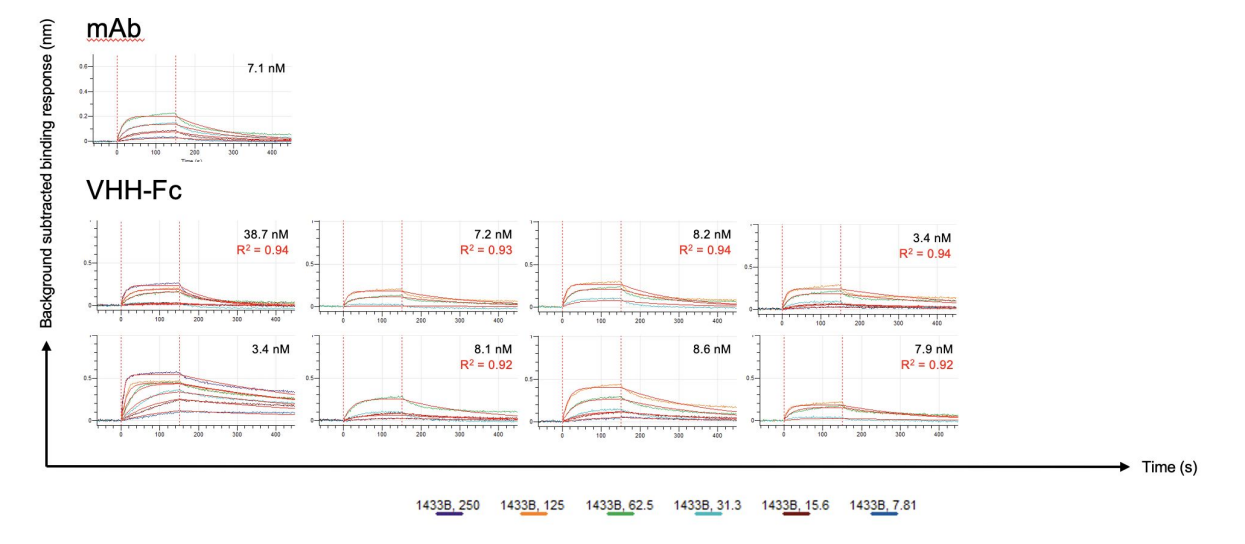
b

UCB9

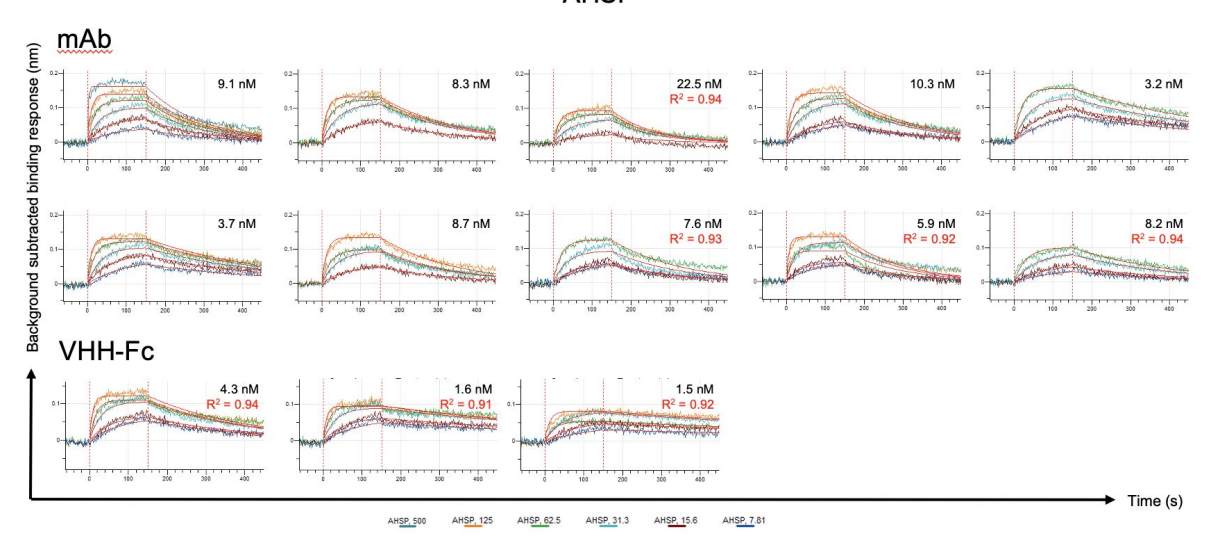


Supp. Fig. 2b. Continued (2/4)



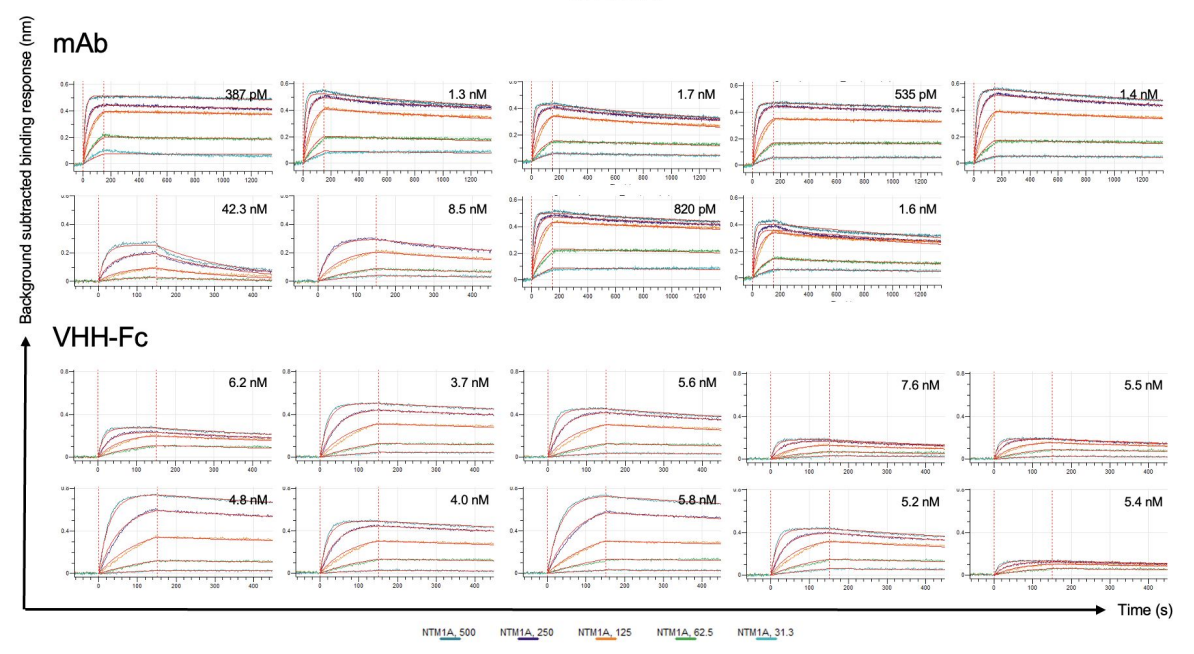


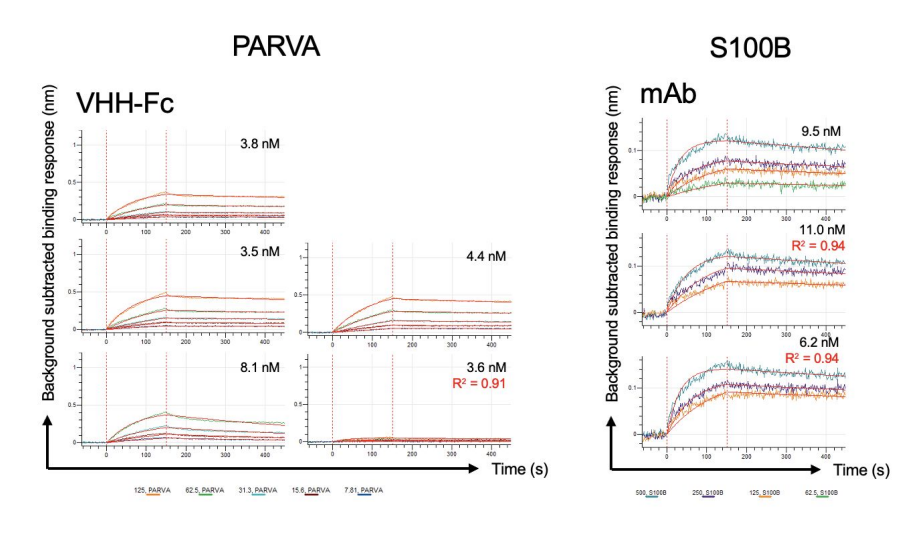
AHSP



Supp. Fig. 2b. Continued (3/4)

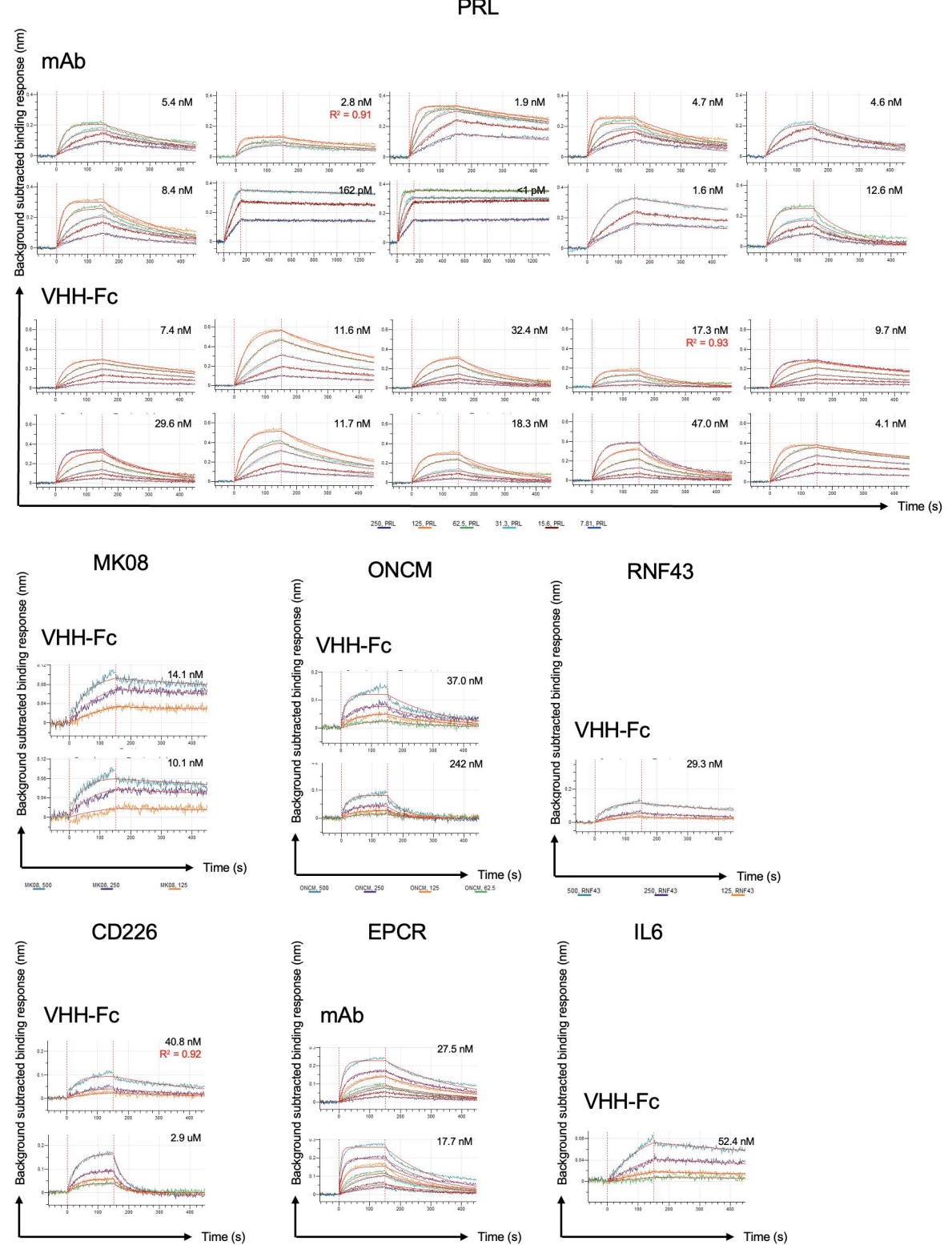


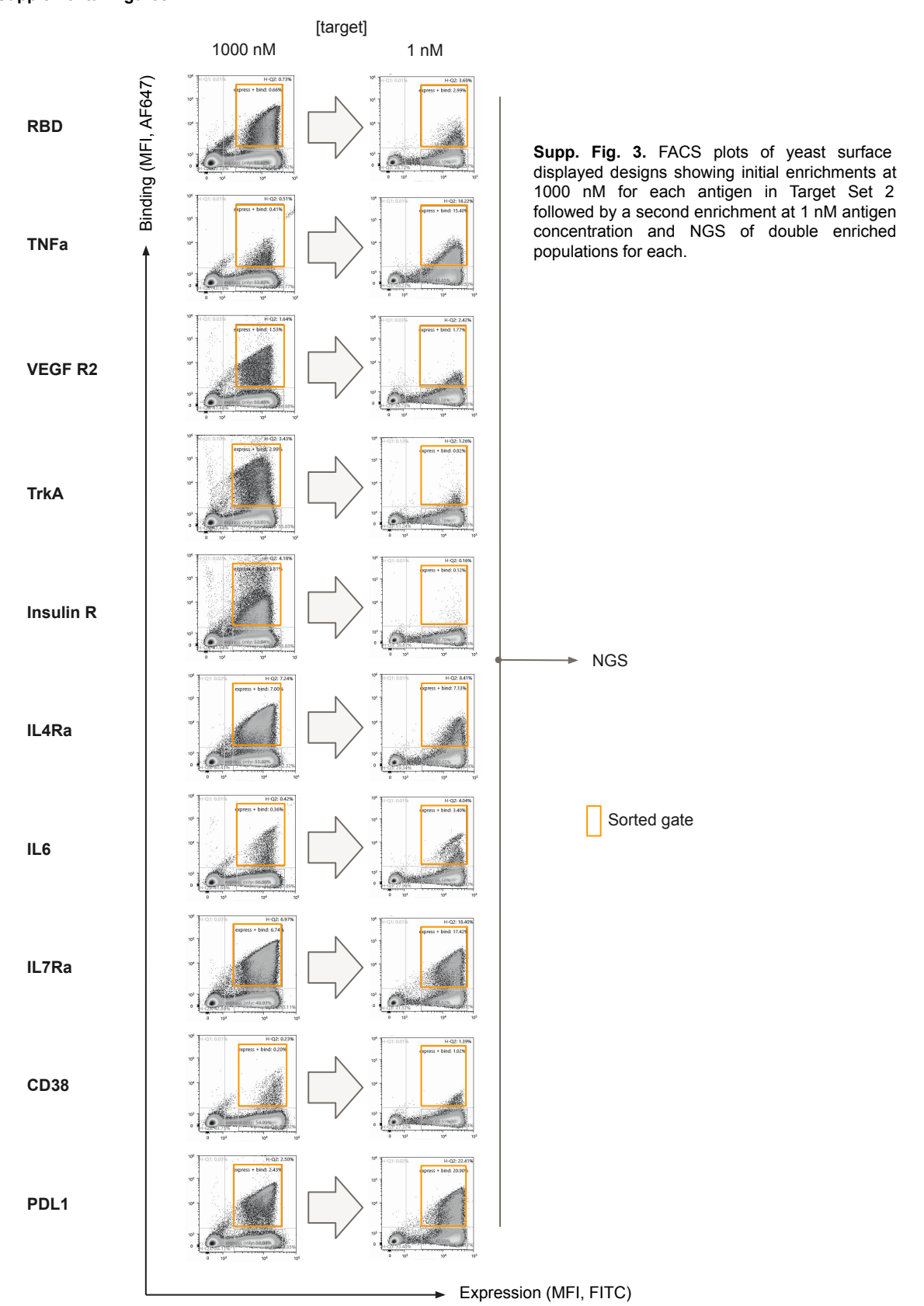




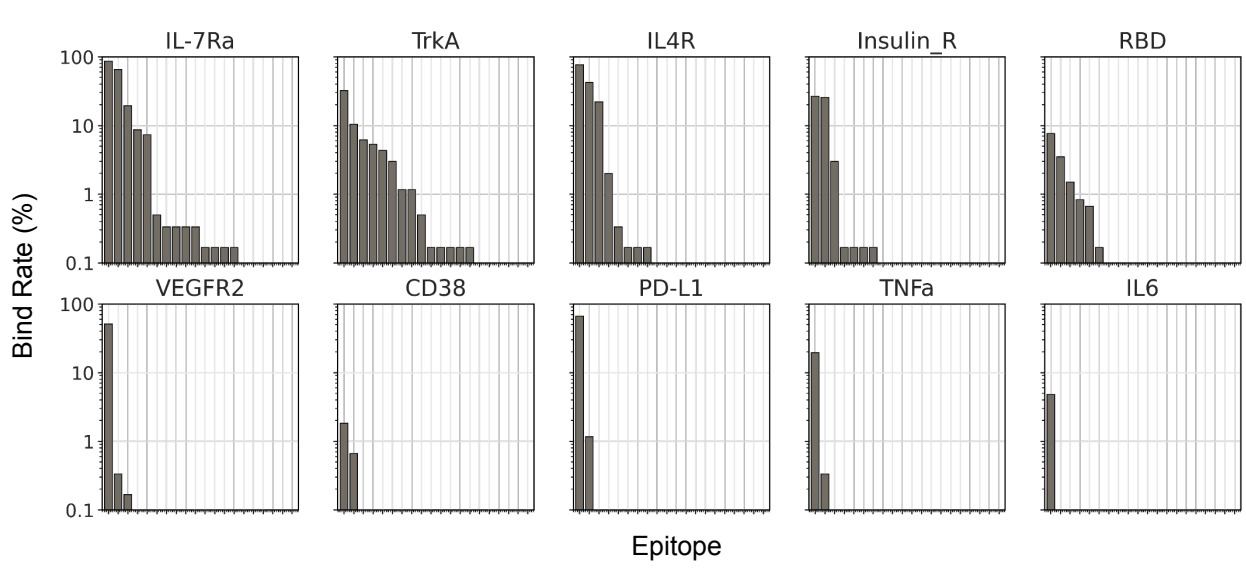
Supp. Fig.2b. Continued (4/4)



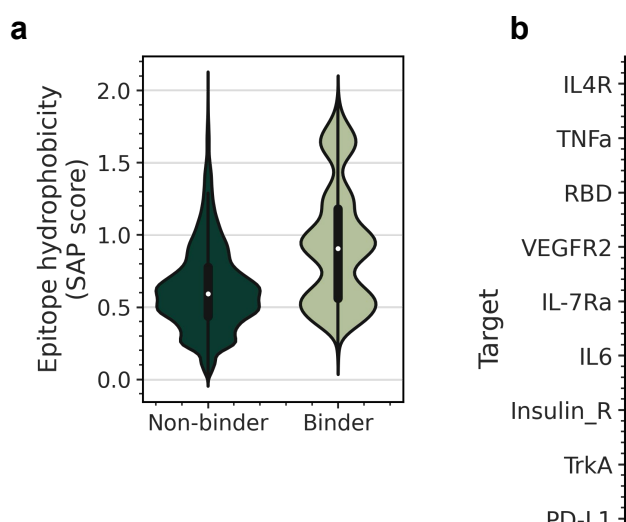


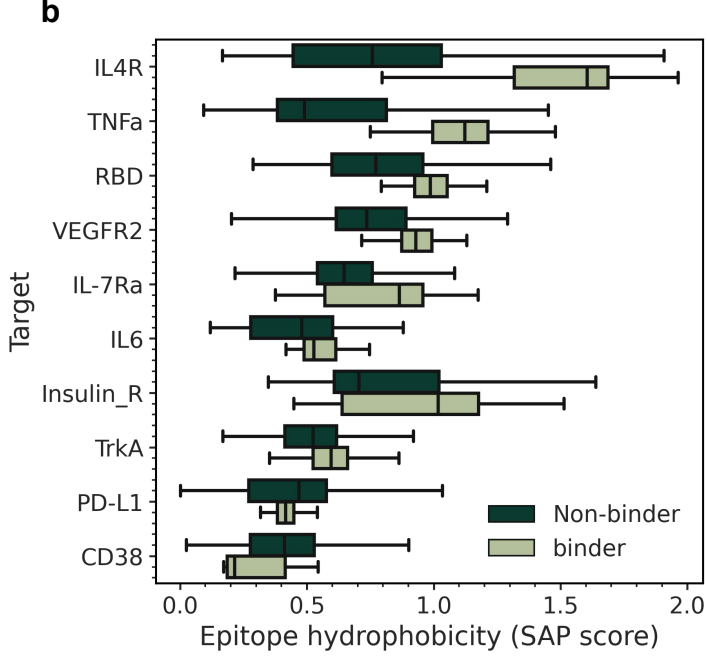


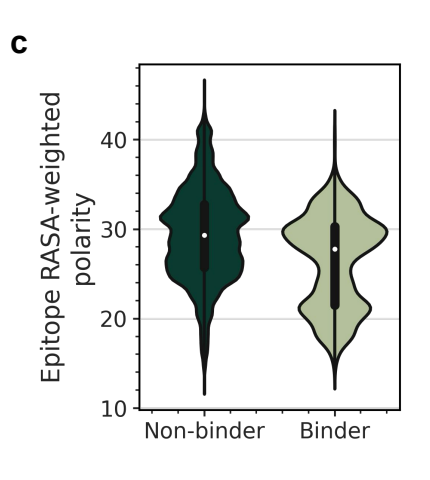
Supp. Fig. 4. Epitope-level bind rates for Target Set 1. For each target subplot, epitopes (bars) are arranged in order of descending bind rate. 20 epitopes were targeted per target.

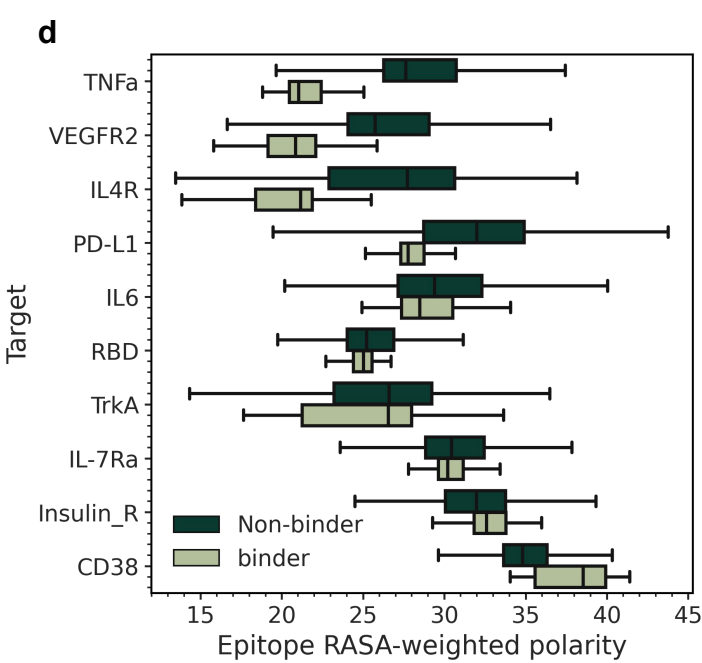


Supp. Fig. 5. *De novo* designed VHH-Fcs are more likely to bind epitopes with higher hydrophobicity and lower polarity. **a.** Distribution of epitope hydrophobicity as measured by SAP score, separated epitopes belonging to binding VHH-Fcs vs. non-binding VHH-Fcs. **b.** Same as (a) but further separated by targets. **c.** Same as (a) but for epitope polarity. This was calculated by computing a weighted average the Zimmerman polarity index of each residue in the epitope, where weights were each residue's relative accessible surface area (RASA) to solvent. **d.** Same as (c) but further separated by targets.



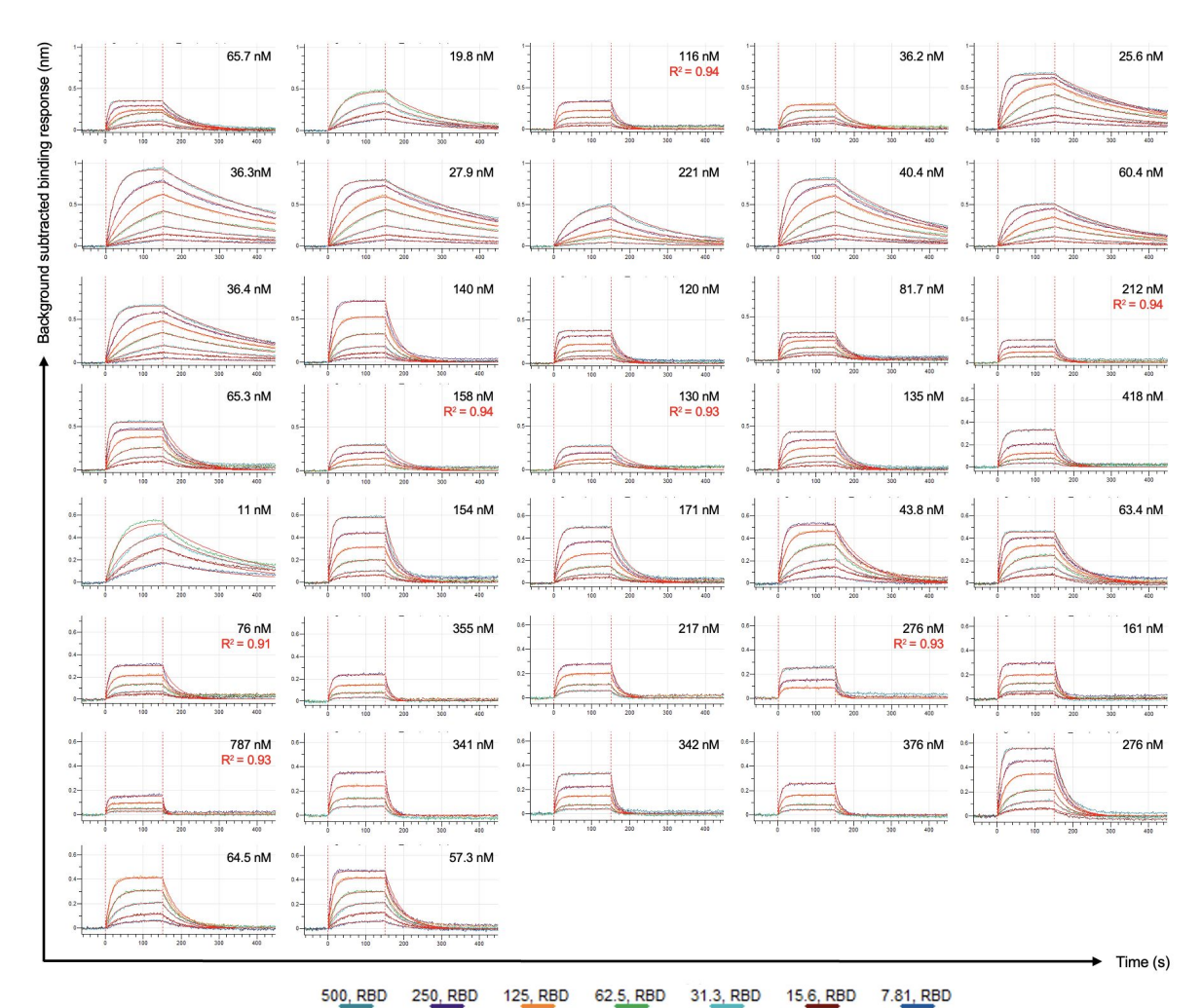






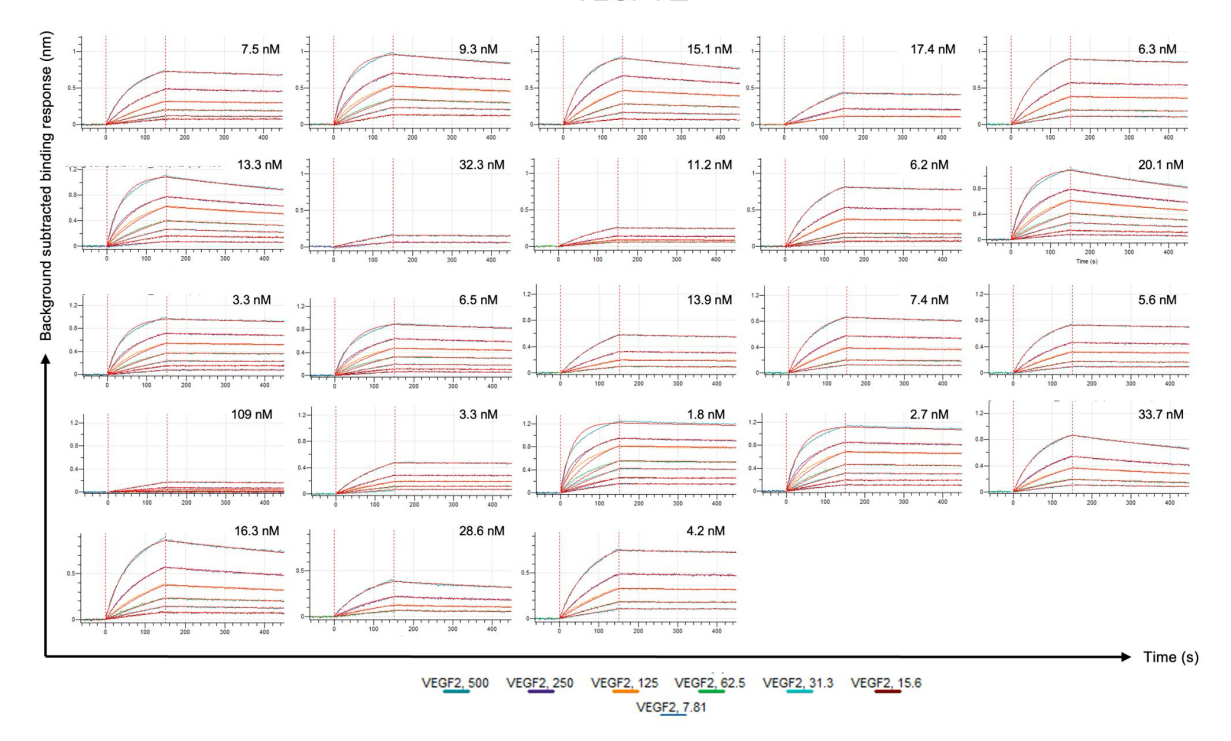
Supp. Fig. 6. BLI kinetic sensograms for JAM-2–designed antibodies binding 10 different antigens from Target Set 2. For each antigen, background-subtracted binding responses are shown for individual VHH-Fc or mAb designs; each panel corresponds to one antibody. Colored curves represent sensorgrams at a series of analyte concentrations (typically 7.8–500 nM), and red curves show global 1:1 Langmuir fits used to determine the apparent K_D, reported above each panel. The y-axis indicates background-subtracted binding response (nm) and the x-axis indicates time (s); vertical dashed lines mark transitions between baseline, association, and dissociation phases. Unless otherwise annotated in red, fits have $R^2 \ge 0.95$. Panels labeled "No confident k_{dis} " or with red R^2 values denote interactions where extremely slow dissociation or lower fit quality prevented a reliable kinetic K_D estimate.



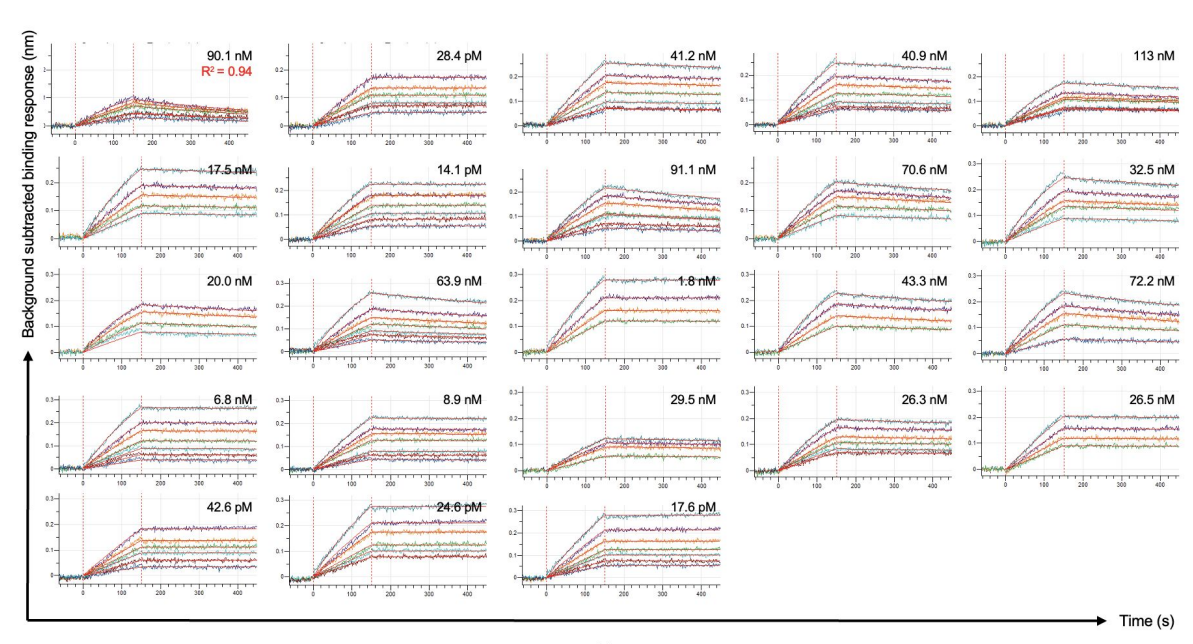


Supp. Fig. 6. Continued (2/8)

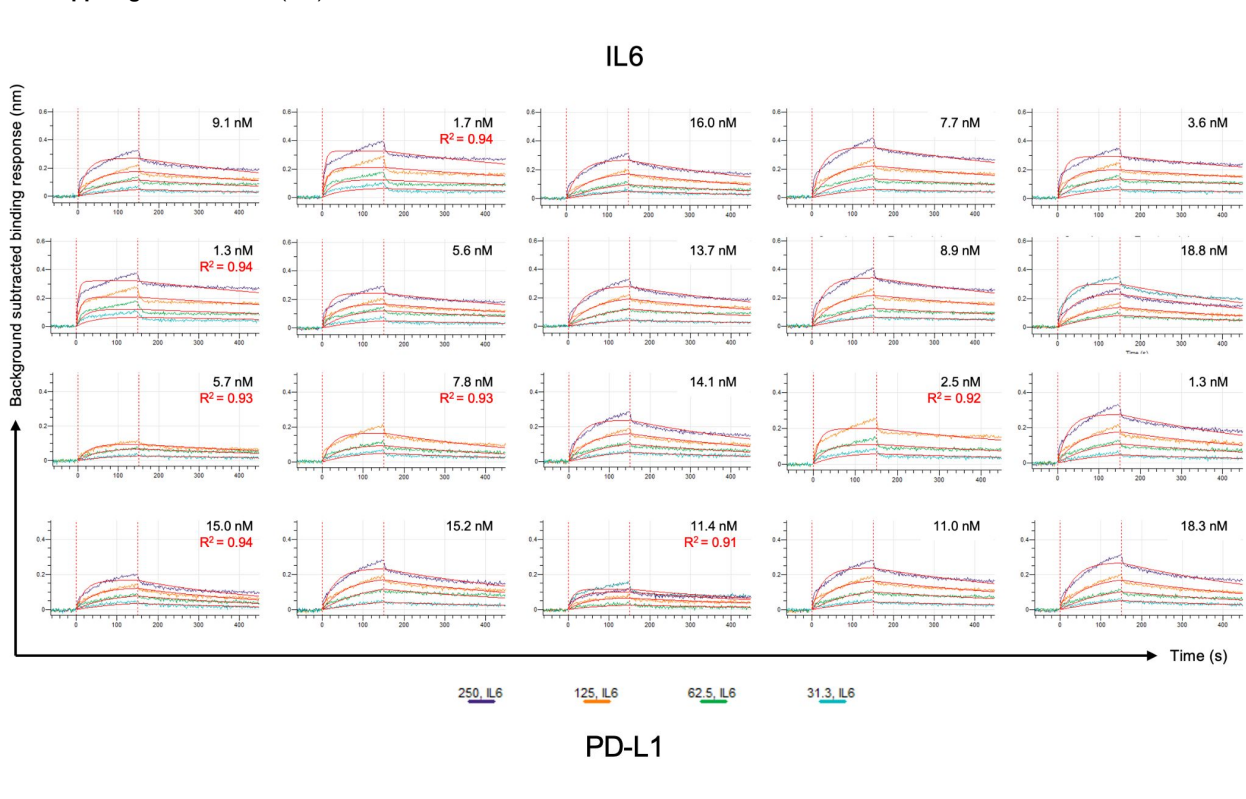


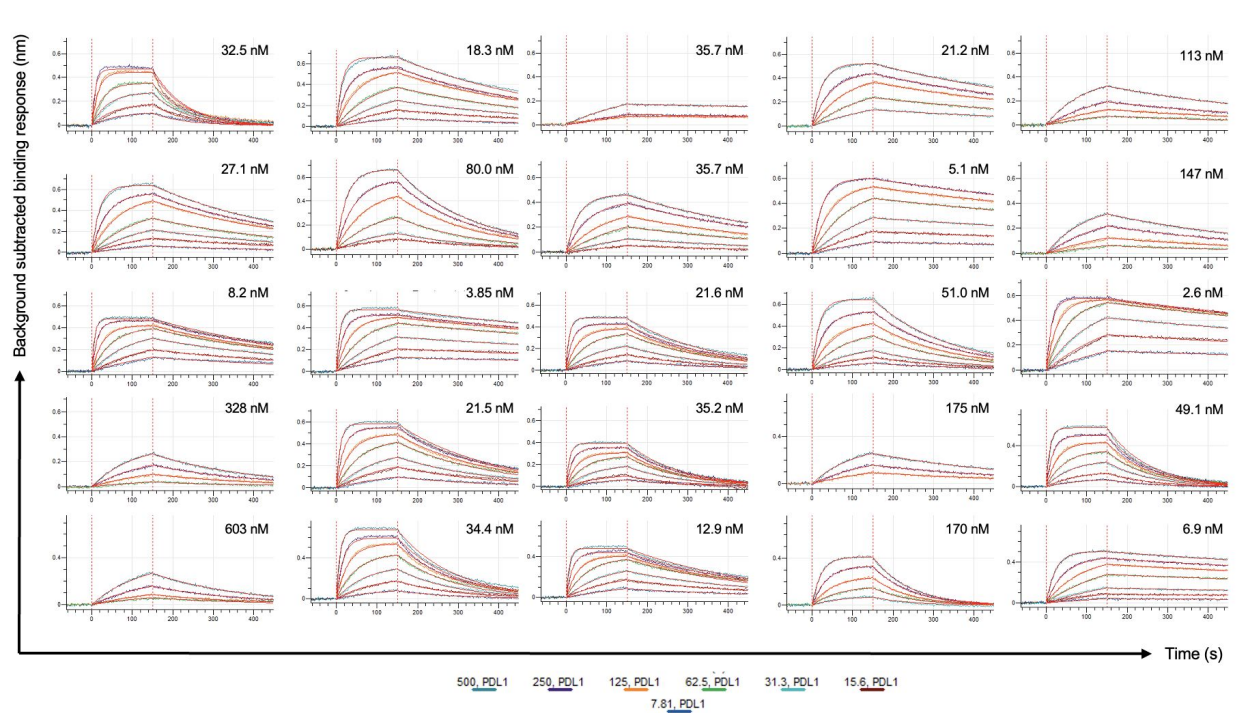


TNFa



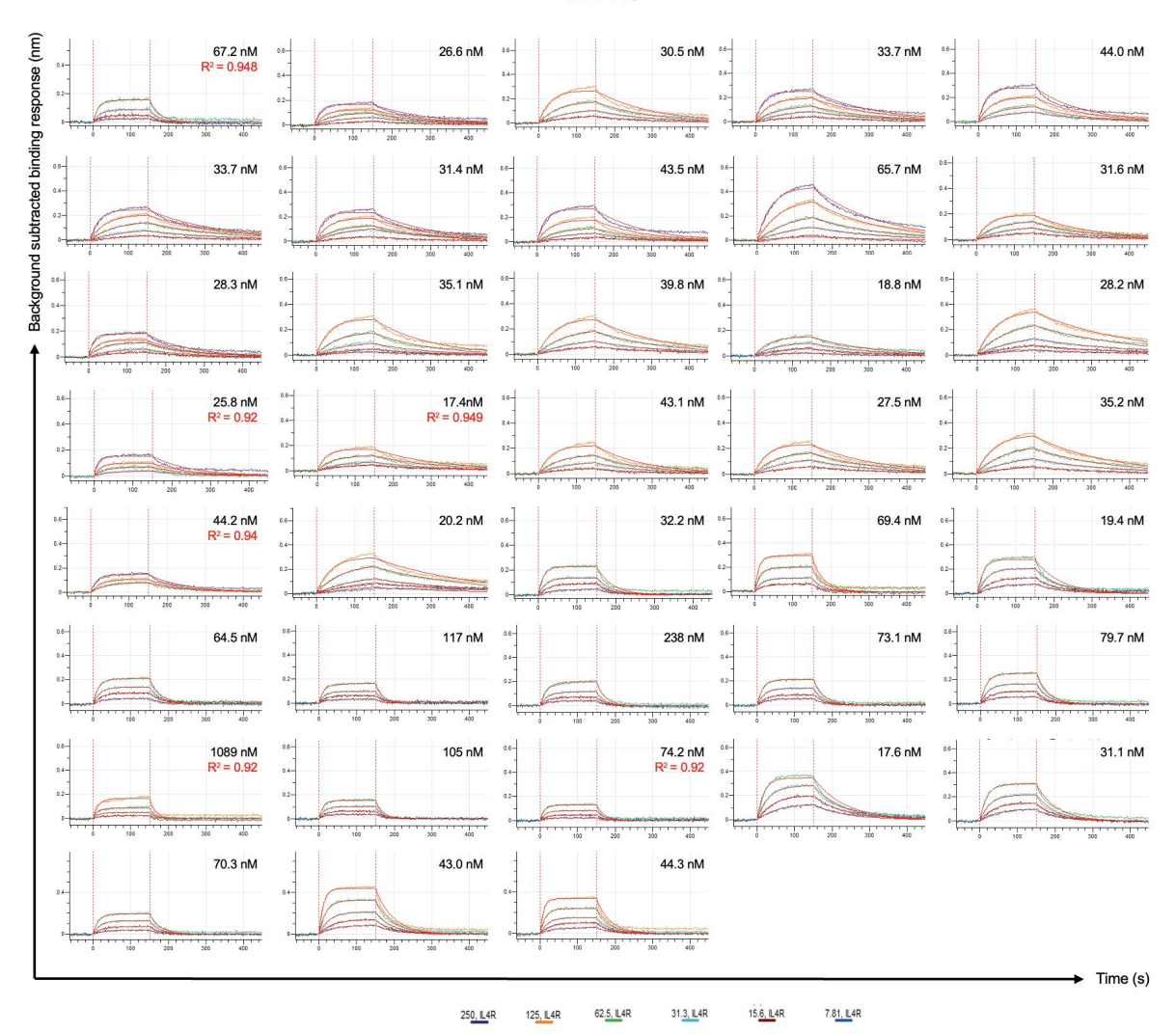
Supp. Fig. 6. Continued (3/8)



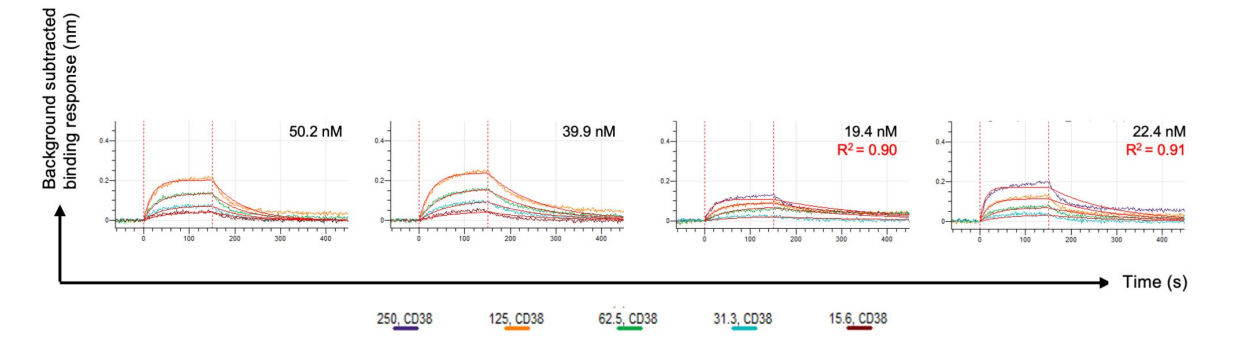


Supp. Fig. 6. Continued (4/8)

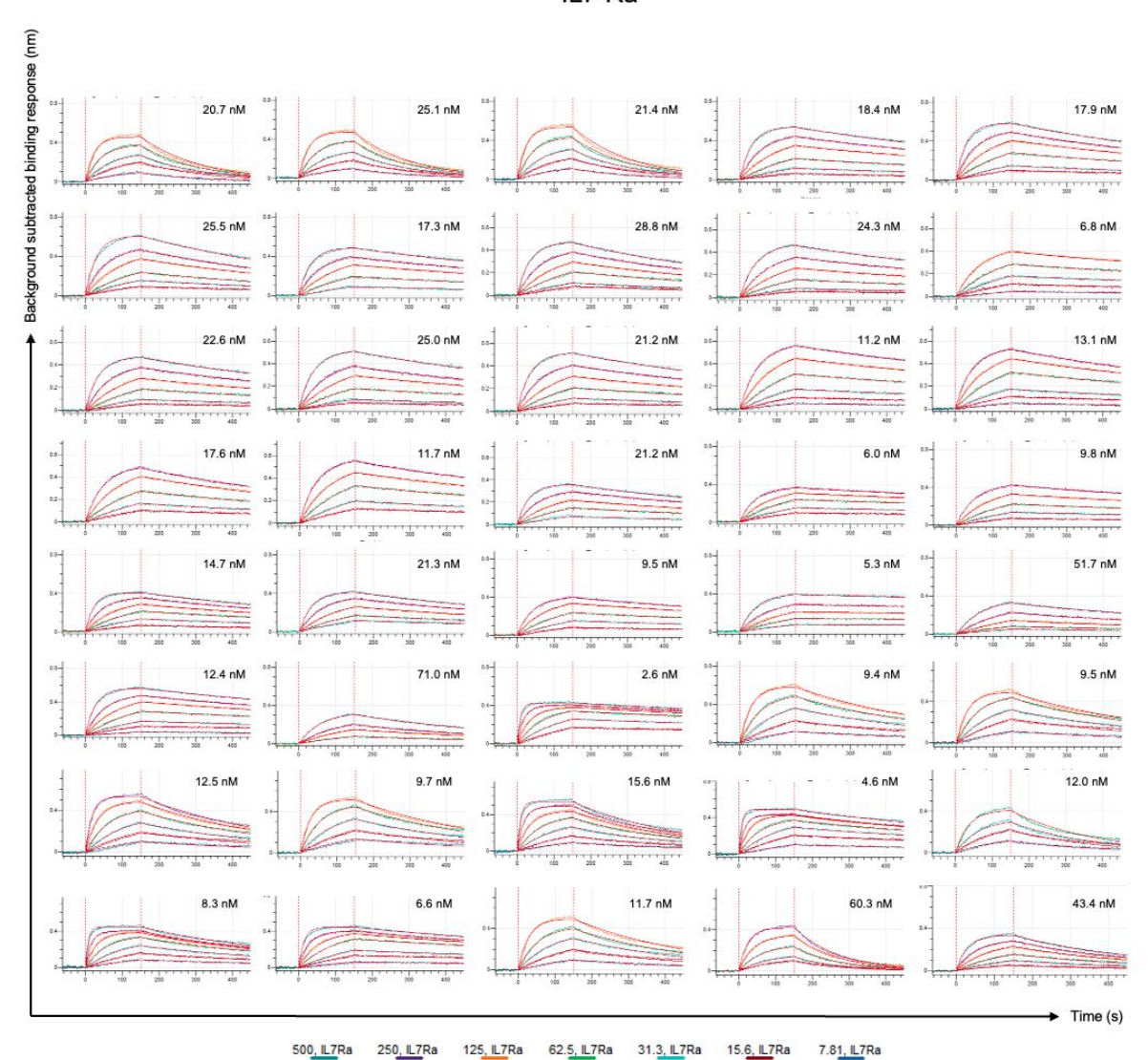




CD38

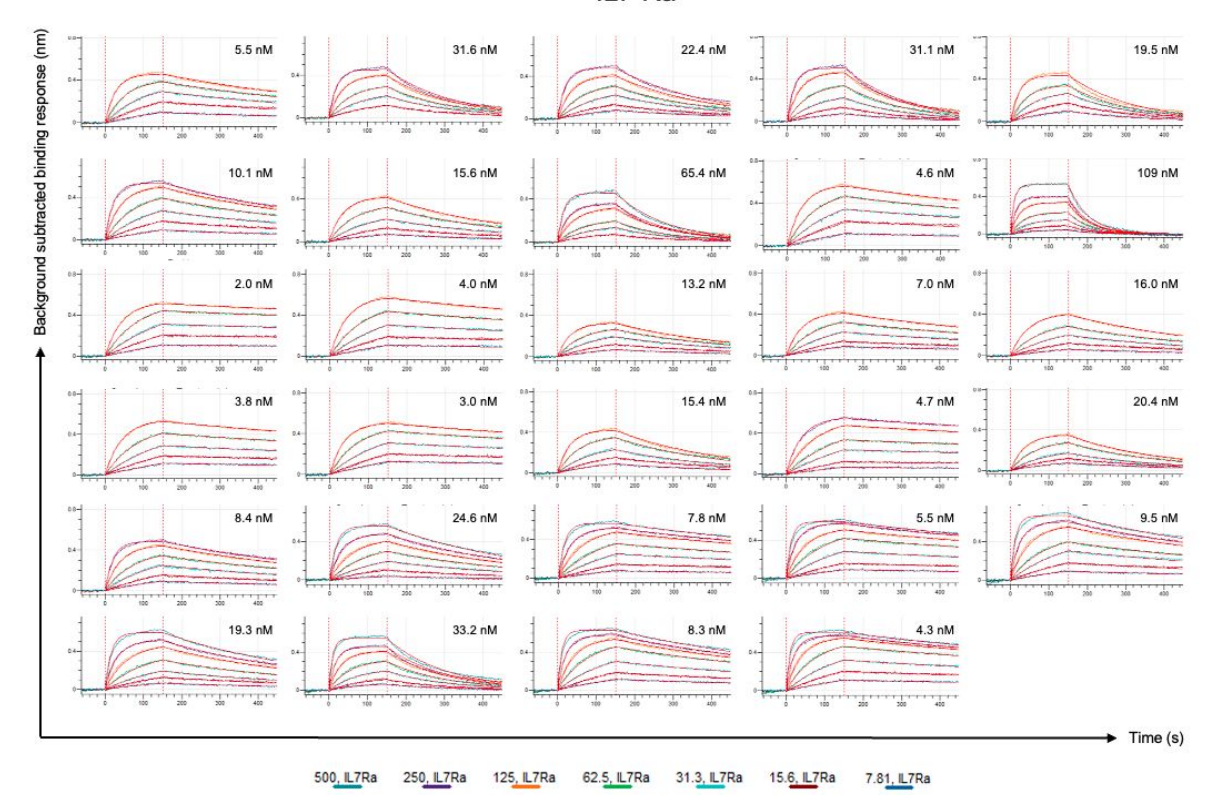


IL7-Ra

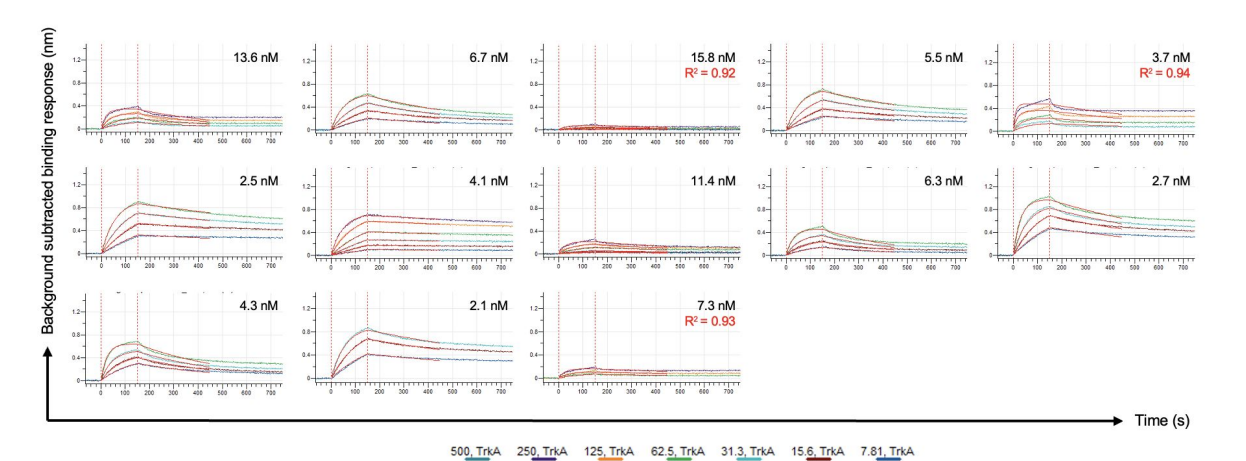


Supp. Fig. 6. Continued (6/8)



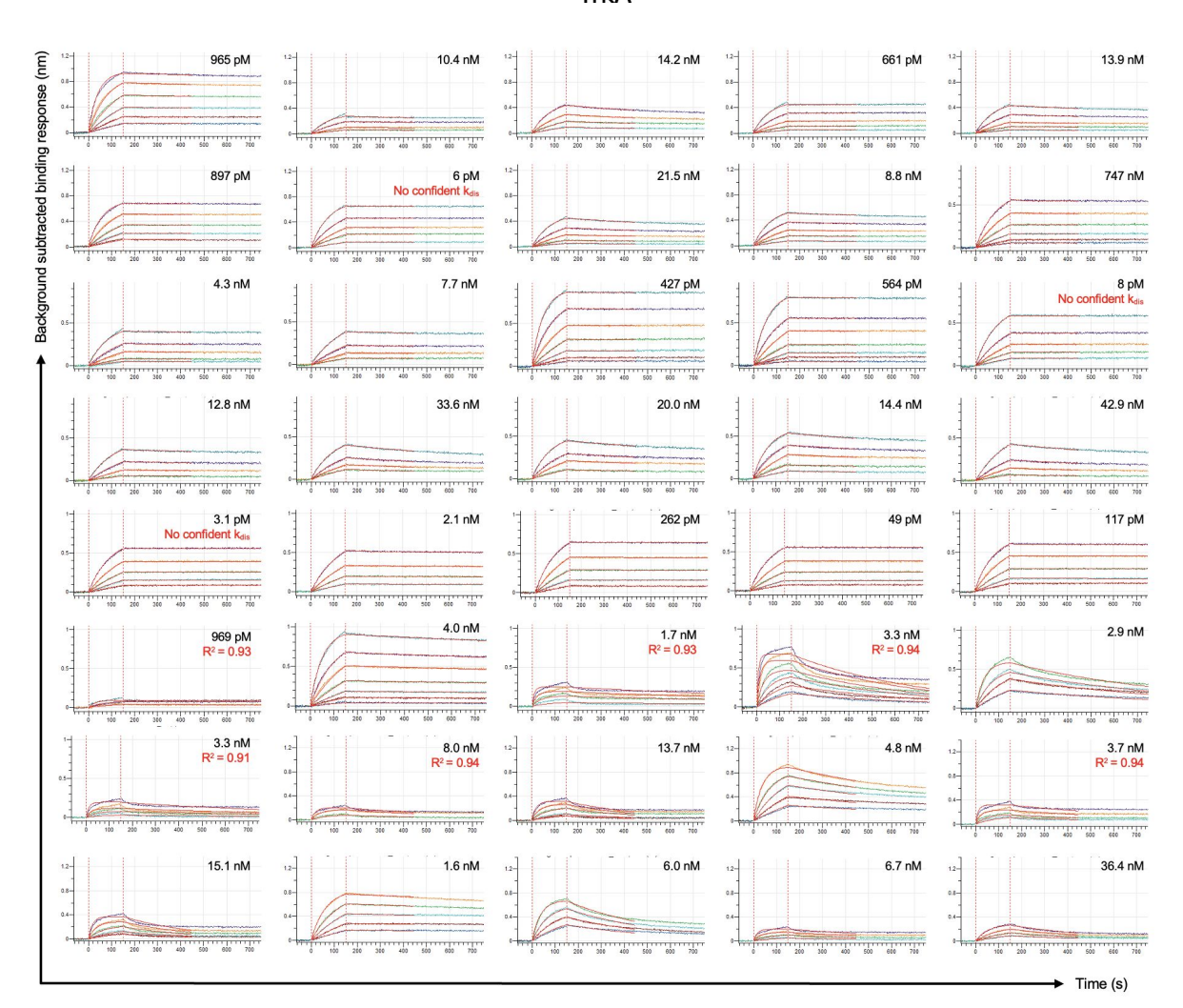


TrkA



Supp. Fig. 6. Continued (7/8)

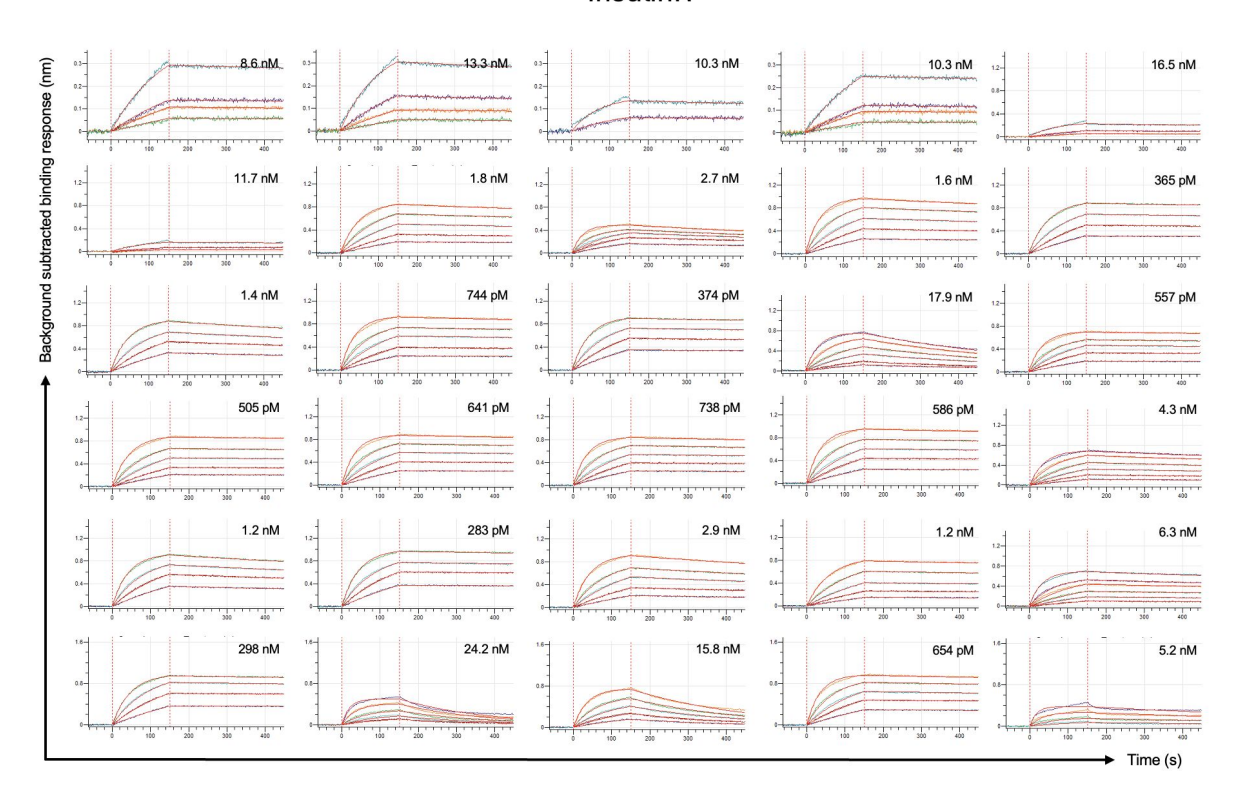
TrkA



500, TrkA 250, TrkA 125, TrkA 62.5, TrkA 31.3, TrkA 15.6, TrkA 7.81, TrkA

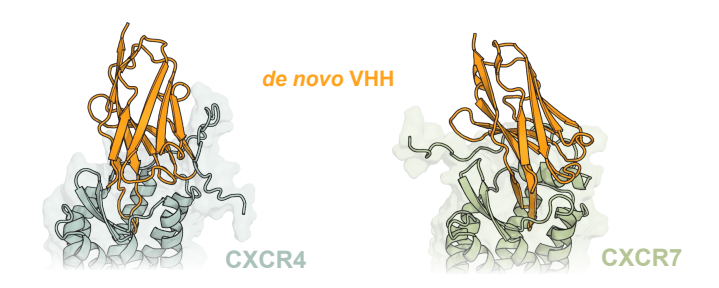
Supp. Fig. 6. Continued (8/8)

InsulinR

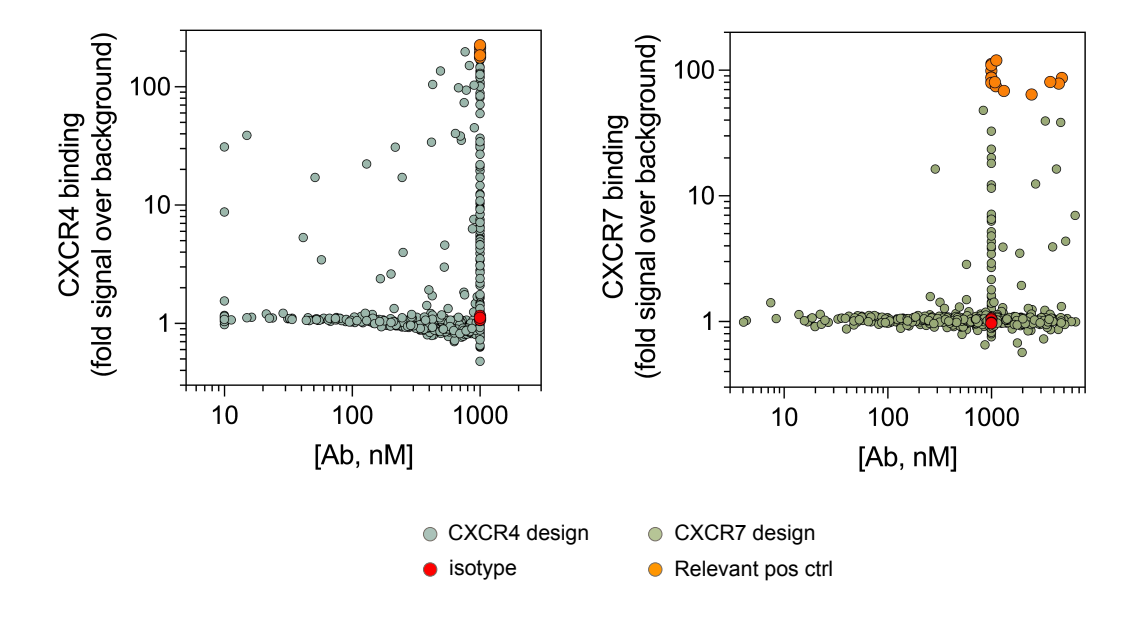


Supplemental Figures

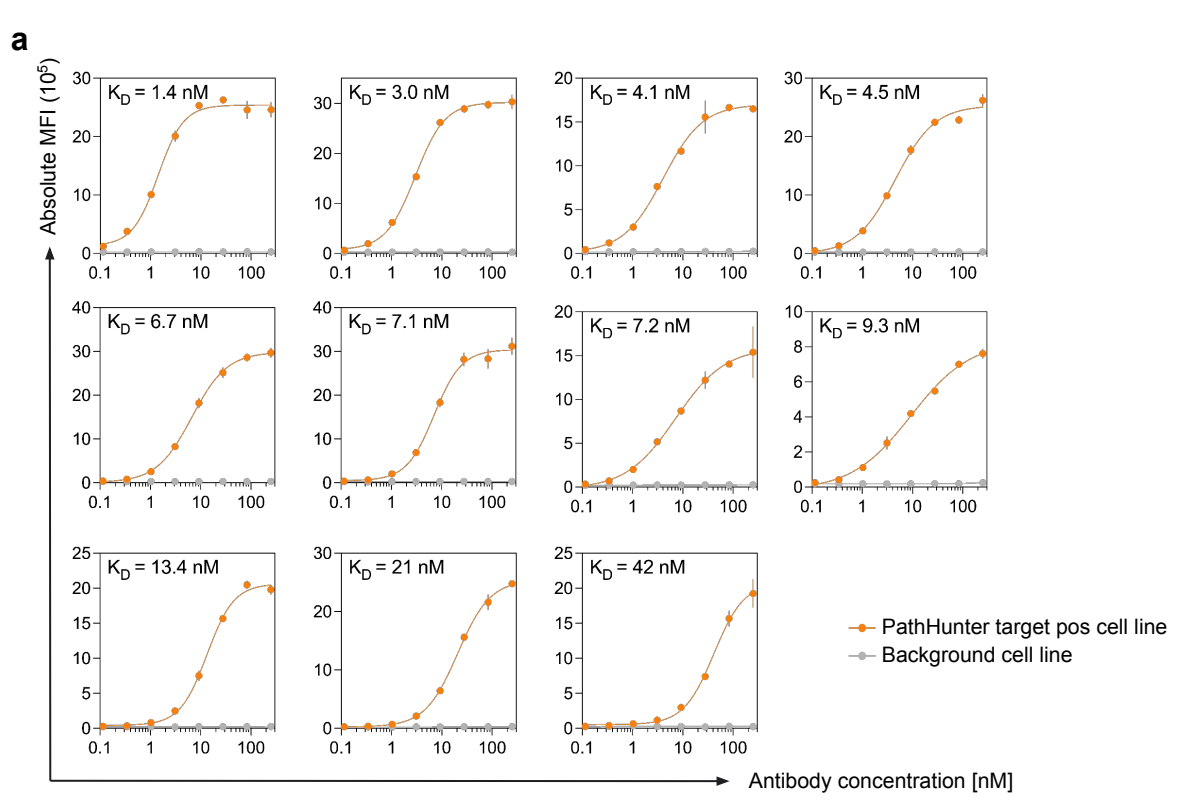
Supp. Fig. 7. JAM-generated complexes of CXCR4 (light blue) and CXCR7 (light green) and each bound by designed VHH antibodies (orange). The designed VHHs target the orthosteric binding site of the GPCR



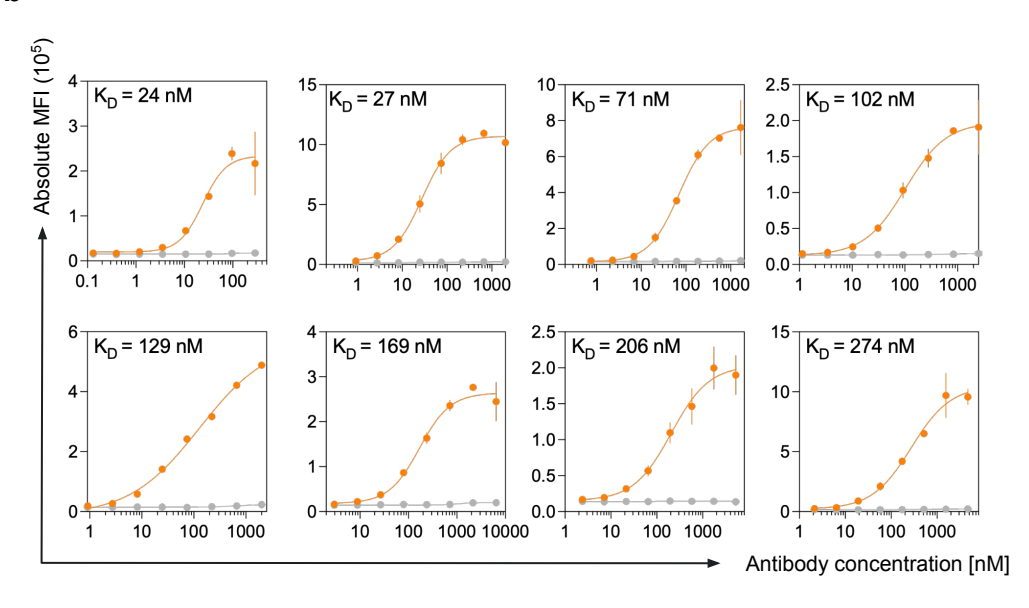
Supp. Fig. 8. Single-point cell-binding screen for JAM-2–designed anti-CXCR4 (left) and anti-CXCR7 (right) VHH-Fcs. For each design, fold signal over background (MFI on PathHunter GPCR-expressing cells divided by MFI on the matched parental line) is plotted as a function of antibody concentration up to 1000 nM. Blue or green points represent individual JAM-2 designs, orange points denote benchmark Ablynx VHH controls, and red points denote isotype controls. Binders were defined as designs with ≥3-fold signal over background.



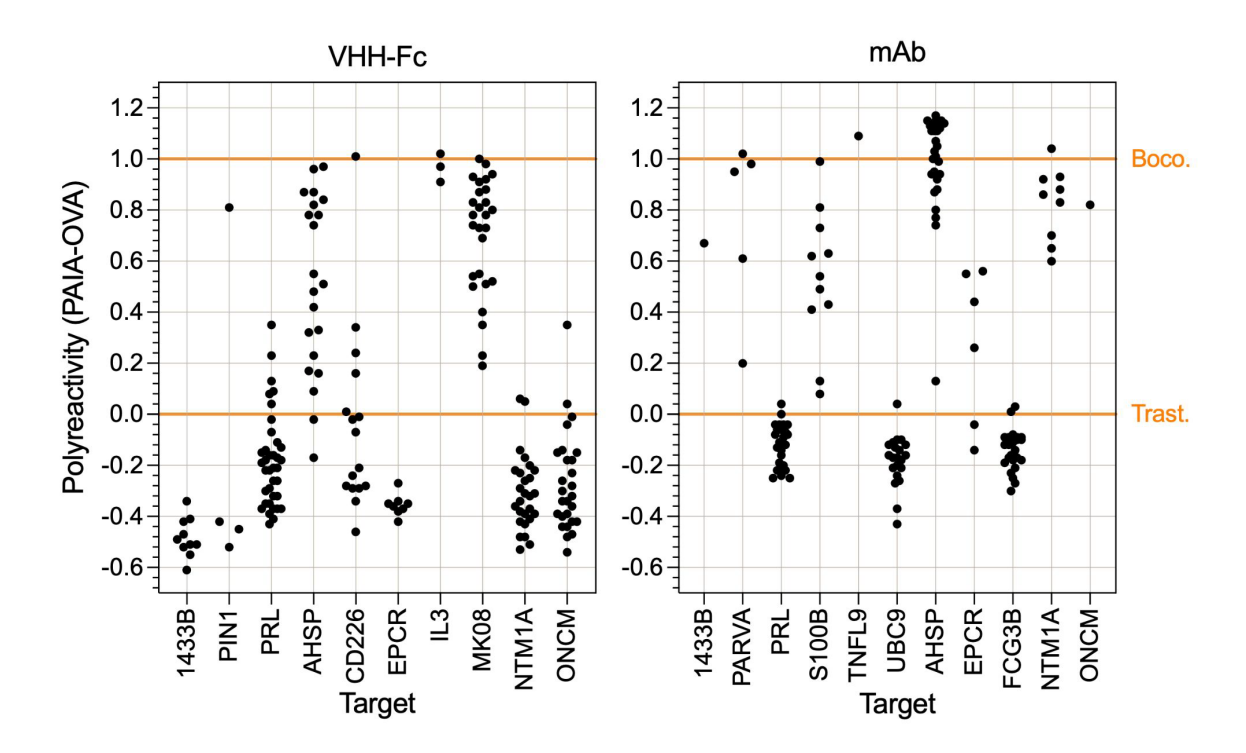
Supp. Fig. 9. Binding traces for all characterized (a) CXCR4 and (b) CXCR7 antibody binders. Error bars are SD. For CXCR4, 11/12 binders are plotted below. The missing twelfth showed an approximate K_n of 110 nM.







Supp. Fig. 10. Polyreactivity of JAM-2–designed antibodies measured by PAIA ovalbumin binding. Normalized PAIA-OVA scores are shown for VHH-Fcs (left) and mAbs (right) across targets; each point represents a single de novo–designed antibody. Values were normalized such that trastuzumab (Trast., lower orange line) corresponds to low polyreactivity and bococizumab (Boco., upper orange line) corresponds to high polyreactivity (lower is better).



Supp. Fig. 11. Sequence and structure novelty. (a) Sequence novelty as measured by percent identity to nearest BLAST hit from a combined sequence database containing all sequences from the OAS (OPIG), INDI (NaturalAntibody), and NR (NCBI) databases (>3 billion sequences total). Novelty is computed separately for heavy (mAb V_H domain/VHH full sequence, top) and light chain (mAb V_L domain, bottom). Orange line drawn at 10% dissimilarity. (b) Structure novelty for each de novo antibody-target complex as measured by alpha-carbon RMSD of the full antibody variable domain structure (top), all CDRs (middle), CDR3 region (mAb HCDR3/VHH CDR3, bottom) to the binder in the most similar binder-target complex structure in SAbDab (OPIG). Orange line drawn at 10 Å. Briefly, the novelty was computed as follows. The the target chain(s) of the JAM-generated binder-target complex was used as a query to a FoldSeek-based search of SabDab. For each hit, the JAM-generated binder-target complex and the hit complex were aligned on the target chain(s) and the RMSD between the JAM-generated binder and binder chain(s) of the hit complex was calculated. The minimum RMSD structure across hits was taken as the most similar binder-target complex structure. See Methods for full implementation details on sequence and structure novelty calculations.

